Article Type: Original Article

Paleoecology of mid-Neoproterozoic hypersaline environments: biomarker evidence for haloarchaea, methanogens and cyanobacteria

Running title: Neoproterozoic biomarkers from a hypersaline environment

R. Schinteie [1], J. J. Brocks [*]

Research School of Earth Sciences, The Australian National University, Canberra, ACT 2601, Australia

* Corresponding author: J.J. Brocks. Research School of Earth Sciences, The Australian National University, Canberra, ACT 2601, Australia. Email: jochen.brocks@anu.edu.au

1 Present address: CSIRO Energy, Organic and Isotope Geochemistry Laboratory, 11 Julius Avenue, North Ryde, NSW 2113, Australia

Keywords: Precambrian, hypersaline, halophiles, Halobacteria, methylotrophic methanogens, crocetane, PMI, caldarchaeol

ABSTRACT

While numerous studies have examined modern hypersaline ecosystems, their equivalents in the geologic past, particularly in the Precambrian, are poorly understood. In this study,

biomarkers from ~820 million year (Ma) old evaporites from the Gillen Formation of the mid-Neoproterozoic Bitter Springs Group, central Australia, are investigated to elucidate the antiquity and paleoecology of halophiles. The sediments were composed of alternating laminae of dolomitized microbial mats and up to 90% anhydrite. Solvent extraction of these samples yielded thermally well preserved hydrocarbon biomarkers. The regularly branched C_{25} isoprenoid 2,6,10,14,18-pentamethylicosane, the tail-to-tail linked C_{30} isoprenoid squalane, and breakdown products of the head-to-head linked C_{40} isoprenoid biphytane, were particularly abundant in the most anhydrite rich sediments and mark the oldest current evidence for halophilic archaea. Linear correlations between the concentrations of these isoprenoids (normalized to *n*-alkanes) and the anhydrite/dolomite ratio reveal microbial consortia that fluctuated with changing salinity levels. Halophilic archaea were the dominant organisms during periods of high salinity and gypsum precipitation, while bacteria were prevalent during stages of carbonate deposition. The irregularly-branched C_{25} isoprenoid 2,6,10,15,19-pentamethylicosane (PMI), with a central tail-to-tail link, was also abundant during periods of elevated salinity, highlighting the activity of methanogens. By contrast, the irregularly-branched C_{20} isoprenoid 2,6,11,15-tetramethylhexadecane (crocetane) was more common in dolomite-rich facies, revealing that an alternate group of archaea was active during less saline periods. Elevated concentrations of isotopically depleted heptadecane (*n*-C_{17}) revealed the presence of cyanobacteria under all salinity regimes. The combination of biomarkers in the mid-Neoproterozoic Gillen Formation resembles lipid compositions from modern hypersaline cyanobacterial mats, pointing to a community composition that remained broadly constant since at least the Neoproterozoic. However, as a major contrast to most modern hypersaline environments, the Gillen evaporites did not yield any evidence for algae or other eukaryotes.

INTRODUCTION

Hypersaline environments are settings where microorganisms, known as halophiles, live under salinity concentrations exceeding those of seawater (e.g., Javor, 1989; Russell, 1992; Oren, 2002). Such environments pose special challenges to life, and organisms adapted to these

settings have evolved mechanisms to cope with these difficulties. Contemporary hypersaline environments host diverse and productive ecosystems encompassing a range of metabolisms and featuring members from all domains of life (e.g., Jahnke et al., 2008; Orphan et al., 2008; Bühring et al., 2009; Heidelberg et al., 2013; García-Maldonado et al., 2015). In such settings, the activity of grazing organisms is suppressed by elevated salinity levels, allowing for the establishment of relatively thick microbial mats. Extensive microbial mats were a dominant sedimentary feature in the Precambrian (> 541 Ma) before the evolution of grazing organisms and numerous studies have characterized modern hypersaline mats to understand the ecology of Precambrian mats (e.g., Hoehler et al., 2001; Bühring et al., 2009). These interpretations rely on the uniformitarian assumption that the biotic composition of ancient hypersaline microbial mats were similar to those of today. However, this hypothesis is difficult to test as the only group of organisms that left a diagnostic microfossil record in Precambrian hypersaline sedimentary facies are cyanobacteria (Oehler et al., 1979; Knoll, 1985). Consequently, the antiquity of different groups of halophiles and the community composition of Precambrian hypersaline ecosystems remain poorly understood.

An alternative approach to studying the microbiology of ancient hypersaline settings is through biomarkers, the hydrocarbon fossils of biological lipids. Biomarkers can be preserved in sedimentary rocks for hundreds of millions of years and many are diagnostic for specific groups of organisms or environmental settings. Some biomarker patterns are diagnostic of hypersaline conditions and have helped to understand the microbial composition of Phanerozoic hypersaline environments (e.g., McKirdy & Kantsler, 1980; ten Haven et al., 1985; Grice et al., 1998; Turich & Freeman, 2011). However, there is no detailed biomarker work on older hypersaline settings and only few studies attributed biomarkers to a hypersaline biota in Precambrian deposits (e.g., Summons et al., 1988a). An ideal target for the search of such biomarkers are the sediments of the ~820 Ma Gillen Formation of the Neoproterozoic Bitter Springs Group in central Australia. The Gillen Formation has played a central role in understanding the evolution of seawater chemistry on the basis of the mineral precipitation sequence that ranges from carbonates to gypsum ± anhydrite to halite. Since the order of these precipitates is the same as that observed in modern equivalents, it was possible to deduce that

the major ion chemistry of seawater at that time was not too different from the present (Holland, 1984). Primary fluid inclusions from mid-Neoproterozoic halite have also shown that the relative concentrations of most major ions are within the range of Phanerozoic seawater (Spear et al., 2014). Furthermore, evaporites of the Gillen Formation fall into the eventful mid-Neoproterozoic time interval (~850 to 635 Ma) that witnessed tremendous environmental and biotic changes, including the first massive Neoproterozoic perturbation of the carbon isotopic record (Bitter Springs Stage Excursion; e.g., Halverson et al., 2007; Klaebe et al., 2016), low-latitude glaciations (Snowball Earth events; e.g., Hoffman et al., 1998), followed by a shift from dominantly anoxic oceans to the modern state of well-oxygenated waters (Sahoo et al., 2012). Here we present biomarkers from ~820 Ma old hypersaline environments, including dolomitized microbial mats, deposited just prior to the Bitter Springs stage excursion, and provide a comparison with modern halophilic ecosystems.

MATERIALS AND METHODS

Geologic setting and sample collection

Study samples record evaporitic, hypersaline conditions and originate from the ~820 Ma Gillen Formation of the mid-Neoproterozoic Bitter Springs Group, Amadeus Basin, central Australia. The Amadeus Basin is one of several Neoproterozoic depocenters in the larger Centralian Superbasin (Fig. 1; Walter et al., 1995; Skotnicki et al., 2008; Edgoose, 2012). Extensive evaporite deposition (100 to > 2000 m in thickness) occurred due to a tenuous connection with the contemporaneous ocean and the shallow nature of the basin (Stewart, 1979; Holland, 1984; Lindsay, 1987; Hill et al., 2000). Evaporite deposition was cyclic and followed patterns also identified in other major evaporite basins. Carbonates and sulfates were deposited closer to the basin margin, while later stage halite and possibly potassium salts were deposited toward the basin center (Lindsay, 1987).

All samples for this study originated from the *Mt Charlotte 1* core held in storage at Geoscience Australia (Canberra) and the Northern Territory Geological Survey (Alice Springs). The core was drilled in the southeastern part of the Amadeus Basin between 1964 and 1965 at

latitude 24°53’41”S and longitude 133°59’11”E (McTaggart et al., 1965; Schmerber & Ozimic, 1966). Eleven samples chosen for this study consisted principally of laminated dolomite and anhydrite with minor siliciclastic content (Fig. 1C-H; Table 1). These samples occurred in sections of the core featuring dolomitized laminae, intraclasts, halite, gypsum ± anhydrite, an input of angular detritus, and red beds. These sedimentary features, taken in combination, point to a shallow marine depositional environment. In modern hypersaline environments, cyanobacteria-dominated mats can enhance dolomite precipitation either through metabolic activity or by providing dolomite nucleation sites on cellular surfaces and exopolymeric substances (e.g., Gerdes et al., 2000; Bontognali et al., 2010). Schinteie (2011) interpreted the Gillen Formation dolomite laminae as fossil microbial mats based on: (1) evidence for cohesive dolomitized layers that resemble modern mat structures; (2) characteristics of low-temperature dolomite precipitation (e.g., Bontognali et al., 2010); and (3) shape, distribution and association of clay and organic-rich laminae with dolomite crystals. Anhydrite crystals are euhedral and form either a polygonal mosaic of equidimensional crystals or are tabular or selenitic in shape. The anhydrite is regarded as the diagenetic product of gypsum (Schinteie, 2011).

Assessment of hydrocarbon contamination

To assess hydrocarbon contamination, all surfaces were either trimmed by using a clean precision wafering saw (Buehler Isomet 1000; Illinois, U.S.A; blade thickness 340 µm) or ablated by a tumbler (a modified KG-1 Mini-Sonic tumbler, Diamond Pacific, U.S.A; Jarrett et al., 2013). Concentration differences of organic molecules between exterior and interior rock portions were quantified according to previously published protocols (Brocks et al., 2008; Brocks, 2011). Exterior and interior rock portions were separately crushed to powder, extracted and fractionated. The quantitative evaluation of hydrocarbon concentration differences between rock portions allowed for the detection and removal of contaminants (Schinteie & Brocks, 2014).

Sample preparation and fractionation

Rock samples were ground to powder in an iron puck mill (Rocklabs, Auckland, NZ). Prior to usage, the mill was cleaned by grinding baked-out (600°C/24 h) quartz-rich sand two to three times for 60 s and then subsequently washed with methanol (solvent grade 99.9%, UltimAR®, Mallinckrodt Chemicals, St Louise, MO, USA) and dichloromethane (DCM; solvent grade 99.9%, UltimAR®, Mallinckrodt Chemicals, St Louise, MO, USA). System blanks consisted of baked-out sand (600°C/24 h). Approximately 5 to 30 g of rock powder were extracted with 100% DCM in a Dionex Automated Solvent Extractor. The extracts were reduced to 100 µL under a stream of purified nitrogen gas and separated into saturated, aromatic and polar fractions using column chromatography over 12 g annealed (450°C/24 h) and dry-packed silica gel (Silica Gel 60; 230-400 mesh; EM Science). Saturated hydrocarbons were eluted with 1.5 dead volumes (DV) *n*-hexane, aromatic hydrocarbons with 2 DV *n*-hexane:DCM (1:1 v/v) and polars with 2 DV DCM:methanol (1:1 v/v). An internal standard of 2.3 µg 18-methyleicosanoic acid methyl ester (18-MEME, Ultrascientific, U.S.A) was added to the saturated and aromatic hydrocarbon fractions. An additional 50 ng of d_4-C_{29}-ααα-ethylcholestane (D4; Chiron Laboratories AS) was added to the saturated fraction as an internal standard for metastable reaction monitoring (MRM).

Gas chromatography-mass spectrometry (GC-MS)

GC-MS of the saturate and aromatic fractions was carried out on a Micromass AutoSpec Premier equipped with a 6890 gas chromatograph (Agilent) and a DB-5 MS capillary column (60 m × 0.25 mm i.d., 0.25 µm film thickness) using helium as the carrier gas (1 mL/min). The MS source was operated at 260°C in EI-mode at 70 eV ionization energy and with 8000 V acceleration voltage. Samples were injected in splitless mode into a PTV injector at a constant temperature of 300°C. For full-scan analyses, the GC oven was programmed at 40°C (2 min), heated to 315°C at 4°C/min, with a final hold time of 17 min. The AutoSpec full-scan duration was 0.7 s plus 0.2 s interscan delay over a mass range of 55-600 Da. For MRM, the GC oven was programmed at 60 ˚C (2 min), heated to 100˚C at 8˚C/min, further heated to 315˚C at 4 ˚C/min and held at the final temperature for 34 min. The following ions were measured in parent to daughter transitions: $M^+ \rightarrow$ *m/z* 134, 177, 184, 191, 205, 217 and 231. *n*-Alkanes were

quantified in partial ion chromatograms using *m/z* 85, pristane *m/z* 268, phytane *m/z* 282 and all other isoprenoids in *m/z* 183. All signal areas are uncorrected for differences in response. Where possible, samples were injected in *n*-hexane to avoid chromatographic peak-shape deterioration (Brocks & Hope, 2014).

Silicalite adduction

The aliphatic hydrocarbon fraction (~2-3 mg) was adducted to silicalite activated at 120°C for 1 h. Silicalite was tightly packed into a Pasteur pipette to a height of 4 cm and washed with dry *n*-pentane. The aliphatic fraction was dissolved in a minimum volume of *n*-hexane, applied to the silicalite column and eluted with 4 column volumes of *n*-pentane (West et al., 1990). *n*-Pentane, containing the branched/cyclic components, was removed by evaporation through a gentle nitrogen stream. The silicalite was dissolved in HF (32%) and the released *n*-alkanes were extracted with *n*-pentane (4x).

Carbon isotope analyses

Compound-specific carbon isotopes were measured through gas chromatography-isotopic ratio mass spectroscopy (GC-IRMS) using a Trace GC connected to a CuO/Ni/Pt combustion unit interfaced via a Finnigan GC III to a Finnigan MAT 252 isotope-ratio mass spectrometer. Samples were manually injected on-column using a DB-5 MS capillary column (60 m x 0.32 mm i.d., 0.25 µm film thickness) and helium as the carrier gas (at a constant flow of 2 mL/min). The GC oven was programmed at 40°C for 10 min, heated to 310°C at 4°C/min and held at the final temperature for up to 10 min. Data was acquired and processed using ISODAT version 7. The system was calibrated and corrected for instrument drift by co-injecting internal standards of perdeuterated *n*-alkanes ($C_{16}D_{34}$, $C_{20}D_{42}$, $C_{24}D_{50}$; Chevron) with known isotopic compositions. All $\delta^{13}C$ values are reported relative to the Pee Dee Belemnite (PDB) standard. Isotopic analyses were carried out in duplicates with reported data achieving an error within ±0.5‰. Kerogen carbon isotope values were analyzed through a commercial operator at the Research School of Biological Sciences, Australian National University, Canberra. All samples analyzed for kerogen isotopes consisted of pre-extracted rock powder.

Total organic carbon (TOC), Rock Eval and extract yields

TOC and Rock Eval measurements were performed by Geotech, Perth, Western Australia. Total yields of extracted saturated and aromatic hydrocarbons were measured in ppm (μg/g of rock) and approximated by integration of total GC-MS signals using 18-MEME as the internal standard. Gravimetric analyses were avoided, since solvent removal causes loss of lighter hydrocarbons and residual solvent in bitumen may result in large systematic errors (Brocks et al., 2003a).

X-ray powder diffraction (XRPD)

XRPD was carried out on a SIEMENS D5005 Bragg-Brentano diffractometer equipped with a graphite monochromator and scintillation detector, using CoKα radiation. The scan range was 4 to 85° 2-theta, at a step width of 0.02°, and a scan speed of 1 second per step. Samples were loaded in side-packed sample holders. The results were interpreted using the SIEMENS software package Diffracplus Eva (2003) and quantified using Siroquant V3.

RESULTS

Biomarker syngeneity

Hydrocarbon contaminants in the eleven rock samples of this study were assessed using rigorous protocols (Brocks et al., 2008; Brocks, 2011). As described by Schinteie & Brocks (2014), all Gillen evaporates had their surfaces trimmed or ablated, followed by the quantification of individual hydrocarbons contained in the rock exterior (E) and interior (I). Generally, E/I ratios ≈ 1.0 indicate even spatial distributions of compounds within rock samples, and commonly signify syngeneity (for exceptions, see Brocks, 2011). E/I ratios >> 1.0, indicate surficial contamination and E/I ratios < 1.0 evaporation from rock surfaces. Increasing E/I ratios with increasing molecular mass in homologous series of hydrocarbons such as *n*-alkanes, are caused by chromatographic effects and point towards permeation of compounds from the rock exterior to the interior. In the Gillen Formation, hopanes, benzohopanes, gammacerane, steranes and mono- and triaromatic steroids were commonly detected on sample exteriors. However, these compounds were excluded from any paleoecological interpretations as they

were either absent in rock interiors, exhibited high E/I values or displayed rising E/I values with increasing molecular mass (Schinteie & Brocks, 2014, their Figures 4H and 5C). For other compound classes, a mixed contribution of syngenetic and contaminant hydrocarbons was observed. In samples containing indigenous bitumen, *n*-alkanes and methylalkanes exhibited minor contaminant overprinting based on E/I ratios that either rose slightly above 1.0 with increasing molecular weight or reached a peak at a specific carbon number (e.g. *n*-C_{25}) followed by a drop in E/I concentration ratios towards 1.0 (Schinteie & Brocks, 2014, their Figures 4D and 4E). These largely indigenous but slightly overprinted hydrocarbons also exhibited high relative concentrations of methylalkanes relative to *n*-alkanes, which is typical of Proterozoic samples (e.g., Pawlowska et al., 2013). Such patterns contrast with samples that were severely contaminated, exhibiting steep mass-dependent E/I concentration gradients with up to 9 to 12 times more *n*-alkanes and methylalkanes on the exterior rock portions than in the interior (Schinteie & Brocks, 2014, their Figures 4A and 4B). These samples also lack the high relative concentrations of methylalkanes to *n*-alkanes typical for the Precambrian (Schinteie & Brocks, 2014, cf. their Figures 5A with 5C). Moreover, based on E/I experiments, a proportion of pristane and phytane as well as all regular, head-to-tail linked isoprenoids > C_{25} were identified as contaminants. Conversely, regular isoprenoid homologues between C_{21} and C_{25} and all irregularly branched isoprenoids are interpreted as syngenetic based on E/I ratios ≈ 1.0 and absence of chromatographic E/I gradients. Based on the E/I data, 54 of 65 samples were excluded from this study as they were pervasively contaminated with allochthonous hydrocarbons (Schinteie & Brocks, 2014). The remaining eleven rock samples were largely sealed against permeation of contaminants and showed no, or only minimal contamination in the interior. Based on rigorous assessments of E/I values of individual hydrocarbons in these eleven samples, only indigenous compounds with no or minimal contaminant overprinting were included in this study.

Bulk characteristics

Rock samples consisted of a variety of lithologies (Fig. 1; Table 1), with total kerogen contents ranging from 0.1 to 0.5% (based on TOC of pre-extracted rock). Total yields of extracted saturated and aromatic hydrocarbons were measured in ppm (μg/g of rock; Table 1).

Groups of hydrocarbon signatures

Three representative GC patterns of saturated hydrocarbon fractions from the Gillen Formation extracts are shown in Figure 2. The first pattern is characterized by high concentrations of mono- (MMA) and dimethyl- (DMA) alkanes relative to *n*-alkanes, a very high unresolved complex mixture (UCM) and low relative abundances of most acyclic isoprenoids (Fig. 2A). This pattern originates from dark-colored rocks with relatively low concentrations of anhydrite but higher abundances of dolomite and siliciclastics. The second pattern also exhibits high relative concentrations of MMA and DMA, but has significantly higher concentrations of regular and irregular (tail-to-tail and head-to-head linked) isoprenoids (Fig. 2B). This pattern originates from rocks that contain a higher proportion of anhydrite but where dolomite is still present in the form of flat, twisted or deformed laminae. The third pattern is characterized by low MMA, DMA and UCM and high relative concentrations of regular isoprenoids (Fig. 2C). This signature originates from samples predominantly composed of anhydrite with little dolomite.

***n*-alkanes and cyclohexylalkanes**

n-Alkanes with chain lengths from 9 to 37 carbon atoms were detected under full-scan GC-MS conditions (Fig. 2). Their distribution is unimodal with a maximum at C_{14} or C_{15}. Apparent in most samples was the elevated concentration of *n*-C_{17} relative to *n*-C_{16} and *n*-C_{18}. Separation of *n*-alkanes from isoprenoids through silicalite adduction indicated that the elevated concentration of *n*-C_{17} is genuine and not caused by co-elution. Alkanes possessing a terminal cyclohexyl ring were also detected in all *m/z* 83 partial mass chromatograms.

Monomethyl- (MMA) and dimethylalkanes (DMA)

As described above, MMAs are strongly elevated relative to *n*-alkanes in dolomite-rich samples and typically lower in those composed predominantly of anhydrite (Fig. 2). The dominant MMA

isomers in each homologue cluster are the 3-methyl- (anteiso-) and 2-methyl- (iso-) alkanes. DMAs are also strongly enriched in dolomite-rich samples (Fig. 2) but sharply decline at carbon numbers > C_{17}.

Acyclic isoprenoids

*Regular, head-to-tail linked isoprenoids (*i-C_x*)*

A pseudo-homologous series of regular isoprenoids was detected in *m/z* 183 mass chromatograms in all Gillen samples. However, the range of this series varied depending on host-rock mineralogy. Dolomite-rich samples yielded mostly pristane (Pr = *i*-C_{19}) and phytane (Pr = *i*-C_{20}) and their C_{14} to C_{18} breakdown products (Fig. 2A). Anhydrite-rich samples, by contrast, had a series ranging from *i*-C_{14} to *i*-C_{25} (Fig. 2B,C and Fig. 3A). To quantify the importance of these isoprenoids in samples with different mineral contents, we computed the abundances of selected *i*-C_x compounds relative to the two closest eluting *n*-alkanes, e.g., [*i*-C_{25}] = 2 * *i*-C_{25}/(*n*-C_{22} + *n*-C_{23}), and plotted them against anhydrite content (Fig. 4). A positive, apparently linear correlation was observed between the anhydrite/dolomite ratio and [*i*-C_{25}] (R^2 = 0.87; $p < 0.0001$ Fig. 4B). Moreover, the ratio *i*-C_{25}/Ph showed a weak but significant correlation with anhydrite weight-% (R^2 = 0.59; $p < 0.01$; not shown). By contrast, [pristane], [phytane] and the Pr/Ph ratio did not exhibit any correlations with mineralogy.

In the Gillen evaporites, Pr/Ph ratios range from 0.85 to 1.88 (Table 1). Generally, the Pr/Ph ratio is largely controlled by oxidation and decarboxylation (loss of terminal carbon atom) of a functionalized C_{20} precursor such as phytol. By analogy, it is plausible that *i*-C_{24} is the decarboxylation product of a biogenic C_{25} precursor. To test whether *i*-C_{19} and *i*-C_{24} were generated by similar processes and under comparable diagenetic conditions, Pr/Ph was plotted against *i*-C_{24}/*i*-C_{25}, yielding a strong positive correlation (R^2 = 0.80; $p < 0.0005$; Fig. 5A).

Irregular, tail-to-tail linked isoprenoids

The irregular C_{20} isoprenoid crocetane (2,6,11,15-tetramethylhexadecane), with one central tail-to-tail link, was identified based on comparison with the mass spectrum of authentic crocetane (provided by Steven Rowland, University of Plymouth; Robson, 1987; Robson &

Rowland, 1993) and co-injection experiments (Fig. 3B). Although crocetane and phytane co-elute and have similar mass spectra, the irregular isomer exhibits a more intense *m/z* 169 ion, while phytane has a dominant *m/z* 183 ion (Robson & Rowland, 1993). The ratio of *m/z* 169 to *m/z* 183 thus reflects the approximate relative contributions of these two isomers to the combined crocetane-phytane signal (i.e. crocetane/Ph ≈ *m/z* 169/183). Similar approaches using ion ratios have previously been made to measure the relative abundances of co-eluting compounds (e.g., van Bentum et al., 2012). In this study, a positive correlation was observed between the dolomite content of the eleven evaporite samples and the crocetane/phytane ratio (*m/z* 169/183; $R^2 = 0.74$; $p < 0.001$; Fig. 6A).

The C_{25} isoprenoid 2,6,10,15,19-pentamethylicosane (PMI), with a central tail-to-tail link, was also identified eluting marginally before the regular *i*-C_{25} (2,6,10,14,18-pentamethylicosane). The presence of this irregular isoprenoid was confirmed by co-injection experiments with an extract from a New Zealand Miocene hydrocarbon seep carbonate (provided by Emmanuelle Grosjean, Geoscience Australia; Fig. 3C). While PMI and *i*-C_{25} partially co-elute and have similar mass spectra, the irregular isomer exhibits a higher *m/z* 239/253 ratio than the regular isomer (Risatti et al., 1984). Plotting the *m/z* 239/253 ratio thus reflects the approximate relative abundances of the two isomers (i.e. PMI/*i*-C_{25} ≈ *m/z* 239/253). No correlations were observed between the ratios PMI/*i*-C_{25} and crocetane/phytane, or between PMI/*i*-C_{25} and variations in host rock mineralogy.

The C_{30} tail-to-tail linked isoprenoid squalane was detected in all samples based on its mass spectrum and elution position (Fig. 2). The concentration of squalane relative to *n*-alkanes, [squalane] = 2 * squalane/(*n*-C_{26} + *n*-C_{27}), increased with respect to anhydrite content, following a curved function resembling a hyperbola (Fig. 4C). Plotting [squalane] against the anhydrite/dolomite ratio yielded a strong linear correlation ($R^2 = 0.96$; $p < 0.0000005$; Fig. 4D). Positive correlations also exist between [squalane] and [*i*-C_{25}] ($R^2 = 0.93$; $p < 0.000005$ Fig. 5B), and between [squalane] and PMI/*i*-C_{25}, albeit with a major outlier ($R^2 = 0.76$; $p < 0.005$ after removal of outlier; Fig. 6C). A strong negative correlation was observed between [squalane] and the crocetane/phytane ratio ($R^2 = 0.82$; $p < 0.0005$; Fig. 6B).

Irregular, head-to-head linked isoprenoids

Irregular isoprenoids with a central head-to-head link were detected in ten out of eleven samples in the carbon number range C_{32} to C_{40} (Fig. 2). They were identified by comparison with GC elution positions and mass spectra of the same compound class in a Miocene crude oil from the San Joaquin Basin, California (Fig. 3D; provided by J.M. Moldowan; Moldowan & Seifert, 1979). A strong positive correlation was observed between the relative abundance of the head-to-head linked isoprenoids, [*i*-C_{39}] = 2 * *i*-C_{39}/(*n*-C_{31} + *n*-C_{32}), and the anhydrite content following a curved, hyperbola-like function (Fig. 4E). A plot of [*i*-C_{39}] against the anhydrite/dolomite ratio yielded a strong linear correlation (R^2 = 0.97; $p < 0.00001$; Fig. 4F). Positive linear correlations were also found between [*i*-C_{39}] and [*i*-C_{25}] (R^2 = 0.92; $p < 0.000005$ Fig. 5C), [squalane] (R^2 = 0.93; $p < 0.000005$; not shown) and, after exclusion of one outlier, PMI/*i*-C_{25} (R^2 = 0.66; $p < 0.005$; not shown). A negative correlation was observed between [i-C_{39}] and the crocetane/phytane ratio (R^2 = 0.79; $p < 0.0005$; not shown).

Hopanoids, gammacerane, and steroids

Although initial whole-rock extraction of Gillen evaporites yielded hopanes and steranes, detailed comparison of the rock exterior and interior conclusively demonstrated that these compounds are surficial anthropogenic contaminants (Schinteie & Brocks, 2014). No evidence for indigenous benzohopanes, gammacerane and mono- and triaromatic steroids was observed.

Maturity determination

Diamondoid maturity values

Adamantanes and diamantanes were detected in all samples (Table 1). Identification of these compounds was based on the mass spectra and elution profiles presented in Wingert (1992) and Chen et al. (1996). Collectively, these two groups of molecules are known as diamondoids and may be the products of rearrangement of polycyclic compounds due to thermal stress in the presence of strong Lewis acids (e.g., Chen et al., 1996; Peters et al., 2005a). The methyl adamantane (MA) index (MAI = 1-MA/(1-MA + 2-MA)) and the methyl diamantane (MD) index

366 (MDI = 4-MD/(1-MD + 3-MD + 4-MD)) were used to evaluate the maturity of the Gillen
367 Formation samples. MAI ranged from 51 to 69% and MDI ranged from 33 to 46% (Table 1).
368 These results correspond to vitrinite reflectance equivalent values (R_c) from 1.1 to 1.3% (Chen
369 et al., 1996), indicating that the Gillen samples are in the late-stage oil/mid-stage wet gas
370 formation (cf. Dow, 1977).
371
372 *Aromatic maturity values*
373 Various aromatic maturity indicators were measured for the Gillen evaporites (Table 1). The R_c
374 calculated from the methylphenanthrene distribution fraction (MPDF; Boreham et al., 1988;
375 Kvalheim et al., 1987) ranges from 0.88 to 1.37%, corresponding to late-stage oil/early gas
376 generation (cf. Dow, 1977). R_c for the methylphenanthrene index-1 (MPI-1; Radke et al., 1982a;
377 Boreham et al., 1988) ranges from 0.9 to 1.5%, corresponding to late-stage oil/mid-stage gas
378 generation. Caution needs to be applied when interpreting MPI-1 values as they appear to
379 reach their maximum at an R_c of ~1.7% and then decrease with higher maturities (Radke et al.,
380 1982a; Boreham et al., 1988). This reversal is related to demethylation of methylphenanthrenes
381 to phenanthrene. Reversed MPI-1 values can be recognized by high
382 phenanthrene/methylphenanthrene ratios (Phen/MP > 1; Brocks et al., 2003a). In this study,
383 Phen/MP ratios range from 0.2 to 0.42, indicating that such a reversal did not occur in the
384 Gillen. Another factor that can influence MPI-1 and MPDF values is the kinetically controlled
385 methylation of phenanthrene (Alexander et al., 1995). This process occurs at low temperatures
386 when phenanthrene reacts with methyl donors to yield predominantly 9-methylphenanthrene.
387 Therefore, bitumen with high relative concentrations of phenanthrene might also contain high
388 relative concentrations of 9-methylphenanthrene, resulting in 9-MP/1-MP ratios > 1 and
389 consequently lower MPI-1 and MPDF values (Alexander et al., 1995; Brocks et al., 2003a). In the
390 Gillen samples, the 9-MP/1-MP ratios ranged from 1.68 to 2.07, indicating that such kinetically
391 controlled methylation of phenanthrene may have occurred. However, R_c calculated from MPR
392 (Radke et al., 1982b), which is less affected by methylation reactions (Brocks et al., 2003a),
393 yielded an R_c ranging from 0.89 to 1.59% and in agreement with the other values. Calculation of
394 trimethylnaphthalene ratios (TNR; Alexander et al., 1985; Radke et al., 1986) yielded

comparatively low R_c ranging from 0.83 to 1%, which is still largely placed in the late stage of oil generation. Methyldibenzothiophene ratios (MDR; Radke et al., 1986) were obtained for three samples where methylbenzothiophene concentrations were sufficient and yielded R_c from 0.91 to 1.18%.

Rock Eval, hydrogen, and oxygen indices

Gillen samples did not contain enough organic matter for reliable *Tmax* analysis. Hydrogen (HI = S2/TOC) and oxygen (OI = S3/TOC) indices record very low values (0-50 and 10-50, respectively), and plot close to the origin on a pseudo-van Krevelen diagram (e.g., Tissot & Welte 1984; Peters et al., 2005a). Such low values could be indicative of very high maturity and pose a contradiction to the less mature indicators discussed above. However, the low TOC in these samples is likely giving rise to significantly depressed O and H indices (e.g., Espitalie et al., 1980; Katz, 1983). Therefore, Rock Eval data of the Gillen samples are likely unreliable and will not be discussed further.

Overall maturity of the Gillen samples

Based on the above mentioned proxies, the maturity of the Gillen samples falls into the late-stage of oil (R_c from ~0.8) to mid-stage (R_c to ~1.6%) of gas generation. Therefore, the samples are regarded as thermally mature to highly mature with respect to the oil generation window (cf. Dow, 1977).

Carbon isotope analysis

Compound-specific carbon isotopes of *n*-alkanes and isoprenoids, and bulk carbon isotopes of kerogen show moderate to strong variation in $\delta^{13}C$ within and between samples (Table 2; Fig. 7A). The average carbon isotopic composition of *n*-alkanes range from -21.9 to -27.1‰ (Table 2). In general, $\delta^{13}C$ values become progressively heavier with increasing carbon number from *n*-C_{15} to *n*-C_{21} followed by a drop back to lighter values at higher carbon numbers. The $\delta^{13}C$ of *n*-C_{17} was anomalous, being generally depleted relative to *n*-C_{16} and *n*-C_{18}. $\delta^{13}C$ differences of up to -2.4‰ were recorded between *n*-C_{17} and neighboring homologues (Table 2). A weak but

significant negative correlation was observed when weight percent anhydrite was plotted against average *n*-alkane $\delta^{13}C$ ($R^2 = 0.58$; $p < 0.05$; Fig. 7B). Similarly, a negative correlation was observed when weight-percent anhydrite was plotted against the isotopic depletion of *n*-C_{17} relative to other *n*-alkanes ($\delta^{13}C(n\text{-}C_{17}^*) = \delta^{13}C(n\text{-}C_{17}) - (\delta^{13}C(n\text{-}C_{16}) + \delta^{13}C(n\text{-}C_{18}))/2$) ($R^2 = 0.70$; $p < 0.05$; Fig. 7C).

Compound-specific isotopic analysis of isoprenoids proved difficult due to co-elution. This was particularly the case for phytane and the regular *i*-C_{25} isoprenoid, which co-elute with crocetane and PMI, respectively. Furthermore, a substantial UCM resulted in many isoprenoids being situated on slopes where base-line definitions proved difficult. Thus, Table 2 only lists a small number of values that are reliable. Pristane ranged from -25 to -28‰, phytane+crocetane from -23.9 to -28.9‰, the regular isoprenoid homologues from *i*-C_{23} to *i*-C_{25}+PMI between -24.5 and -28.1‰, and C_{37} to C_{39} head-to-head linked isoprenoids from -25.5 to -26.4‰ (Table 2). Bulk $\delta^{13}C$ of the kerogen ranged from -21.6 to -26.6‰ (Table 2). Such variation was even observed between samples that exhibited similar petrographic textures, mineralogy and near-identical biomarker compositions. A strong linear correlation was observed between the carbon isotopic composition of average *n*-alkanes and kerogen $\delta^{13}C$ ($R^2 = 0.93$, $p < 0.005$; not shown), giving further credence to our methodology for the removal of contaminant hydrocarbons from rock samples (Schinteie & Brocks, 2014). The *n*-alkanes are depleted by 0.3 to 1.6‰ relative to the kerogen, and pristane is 0.4 to 1.2‰ lighter than average *n*-alkanes for the three samples where this could be measured.

DISCUSSON

Interpretation of biomarkers from Gillen Formation evaporites

n-*Heptadecane and other* n-*alkanes*

n-Alkanes are usually the most abundant hydrocarbons in nonbiodegraded oils and mature bitumens. In the Neoproterozoic, these molecules likely originate from various straight-chain molecules such as phospho- and sphingolipids produced by bacteria and eukaryotes (Brocks &

453 Summons, 2004). The lack of detectable steranes in the Gillen samples may indicate that
454 bacteria were the principal source for the *n*-alkanes. The abundance of *n*-alkanes relative to
455 isoprenoids decreases with increasing anhydrite content (Fig. 2). While such a pattern can, in
456 principle, be explained by stage-1 biodegradation of *n*-alkanes, bitumens with low straight
457 chain alkane concentrations also have low MMA, DMA, and UCM abundances, which speaks
458 against this mechanism. Thus, the low *n*-alkane/isoprenoid ratios probably have an ecological
459 explanation, which is discussed further below.

460 In the Gillen samples, $\delta^{13}C$ of *n*-alkanes range from -20.5 to -29.9‰ (Table 2). These values
461 fall within the range reported from *n*-alkanes of ancient Phanerozoic hypersaline settings (e.g.,
462 Grice et al., 1998) and from individual ~820 Ma cyanobacterial fossils of the Bitter Springs
463 Group (-21 to -32‰; House et al., 2000). A prominent feature of most Gillen samples is the
464 elevated concentration of *n*-C_{17}. During early diagenesis, the most common precursors of *n*-C_{17}
465 are presumably C_{17} and C_{18} *n*-alcohols and fatty acids that yield *n*-C_{17} through
466 defunctionalization and carbon loss processes. However, the biogenic carbon number
467 distribution of functionalized *n*-alkyl lipids is often strongly altered in the maturation process
468 with chains cracked or extended and the original carbon number distribution homogenized
469 (Kissin, 1987; Alexander et al., 2011), commonly leaving no trace of the original carbon number
470 preference. In the Gillen, the high relative MMA and DMA abundances and the absence of *n*-
471 alkane carbon preference (except *n*-C_{17}), indicates that these homogenization processes are at
472 an advanced stage. In contrast to functionalized lipids, biologically generated *n*-alkanes (i.e. *n*-
473 alkanes present in living organisms from the outset) are likely more inert to cracking and
474 rearrangement reactions as they lack functional groups required for isomerization processes
475 (Kissin, 1987). Therefore, the most likely precursor for the elevated *n*-C_{17} in the Gillen would
476 have been biologically-produced unfunctionalized *n*-C_{17} itself. Elevated concentrations of *n*-C_{17}
477 have been detected in cyanobacteria and some algae (e.g., Han et al., 1968; Řezanka et al.,
478 1982) and are frequently detected in hypersaline cyanobacterial mats (e.g., Grimalt et al., 1992;
479 Wieland et al., 2008; Bühring et al., 2009) where they are regarded as a marker for these
480 microorganisms. A cyanobacterial source is supported by the carbon isotopic composition of *n*-
481 C_{17}, which is consistently depleted relative to *n*-C_{16} and *n*-C_{18} by up to 2.4‰ (Table 2). The

482 depletion indicates that a fraction of the *n*-C_{17} is derived from a different, isotopically more
483 depleted source than the nearby homologues. Carbon isotopically depleted *n*-C_{17} has been
484 reported from different modern settings and attributed to cyanobacteria (e.g., van der Meer et
485 al., 2000; Kristen et al., 2010). Thus, the elevated abundance of *n*-C_{17} over *n*-C_{16} and *n*-C_{18}
486 coupled with its stronger carbon isotopic depletion, is evidence for the presence of
487 cyanobacteria.

488 Proterozoic hydrocarbons from deep-water sedimentary rocks are distinguished from their
489 Phanerozoic counterparts by ^{13}C enrichment of *n*-alkanes compared to Pr, Ph and bulk
490 sedimentary organic matter (Logan et al., 1995). Logan et al. (1995) suggested that this isotopic
491 enrichment of *n*-alkanes in the Proterozoic resulted from heterotrophic reworking of plankton-
492 derived organic matter in the water column due to the absence of zooplankton and their
493 production of rapidly sedimenting fecal pellets. However, in shallow water, evaporitic
494 environments, $\delta^{13}C$ values for the *n*-alkanes are lighter than kerogen due to limited
495 heterotrophic reworking as organic matter falls a shorter distance followed by rapid burial
496 (Logan et al., 1997, their Table 3 and Figure 7). This observation is in line with that reported
497 here where the average *n*-alkanes from the shallow-water, evaporitic Gillen Formation were
498 slightly depleted in ^{13}C compared to the associated kerogen, and either slightly enriched or
499 depleted relative to C_{19} to C_{39} isoprenoids (Table 2). Additional causes for ^{13}C enrichment of *n*-
500 alkanes in hypersaline environments include (but are not limited to) decreased CO_2 solubility in
501 waters of elevated salinity (Schidlowski et al., 1984; Sumner, 2001) and a high biological
502 productivity in microbial mats (Des Marais et al., 1989; Schidlowski et al., 1994).
503
504 *Cyclohexylalkanes*
505 Low concentrations of cyclohexylalkanes were previously reported in bitumens and petroleums
506 from the Proterozoic and Phanerozoic (e.g., Brocks et al., 2003b). It is conceivable that
507 cyclohexylalkanes could have a direct biologic source in the uncommon *ω*-cyclohexyl fatty acids
508 isolated from some bacteria (Suzuki et al., 1981). However, the close affinity of *n*-alkane and
509 cyclohexylalkane homologue series in rock extracts point to post-depositional cyclization of
510 straight chain lipids as the likely source (Fowler et al., 1986; Hoffmann et al., 1987; Summons et

al., 1988a). Gelin et al. (1994) rationalized the formation of cyclohexylalkanes by allylic cleavage followed by cyclization of aliphatic polyaldehyde.

Methylalkanes

Bitumens extracted from Gillen sediments contain all possible positional MMA isomers with carbon numbers across the full alkane GC elution range (Fig. 2A,B). The distribution of MMA isomers and homologues is similar to typical mature Precambrian and Phanerozoic bitumens. However, the origins of these compounds is still debated, and numerous biogenic and abiogenic factors have been considered.

Suites of methylalkanes have previously been extracted from modern and Holocene-age cyanobacterial mats from hot springs (e.g., Shiea et al., 1990) and sabkhas (Kenig et al., 1995; Kenig, 2000). However, while modern mats generally contain specific positional MMA isomers in the carbon range C_{17} to C_{21} (e.g., Kenig, 2000), mature bitumens generally include all possible positional MMA isomers in comparable abundances and across the full range of detectable carbon numbers (e.g., Fowler & Douglas, 1987; Summons, 1987; Summons et al., 1988a,b). To account for this distribution, Hoering (1981) and Klomp (1986) suggested long-term equilibration of a limited range of positional MMA isomers. By contrast, Kissin (1987) proposed that the full range of MMAs forms through acid-catalyzed migration of methyl-groups along the backbone of *n*-alkenes. The alkenes, in turn, may form by thermal cracking of alkanes or defunctionalization of *n*-alkyl lipids. This mechanism is strongly supported by thermolysis experiments on *n*-alkanes, alkanoic acids and esters in the presence of mineral catalysts, which resulted in mixtures of MMA and DMA closely resembling those found in natural bitumens (Kissin, 1987). Alexander et al. (2011) generated a similar suite of methylalkanes during sealed tube heating experiments of a terminal alkene (1-octadecene) on activated carbon. Therefore, based on the observations of Kissin (1987) and Alexander et al. (2011), the bulk of MMA and DMA isomers and homologues found in mature bitumens, including the Gillen, is interpreted to have formed by abiogenic methyl-transfer and methyl-group migration reactions, and the predominant biogenic precursors are presumably functionalized branched and *n*-alkyl lipids.

An outstanding characteristic of dolomite-rich Gillen evaporites is the high abundance of MMAs and DMAs relative to *n*-alkanes (Fig. 2A,B). This pattern is frequently observed in the Precambrian and Cambrian but less commonly in younger periods (e.g., Fowler & Douglas, 1987; Summons, 1987; Summons et al., 1988a; Pawlowska et al., 2013). The precise reason for these elevated abundances is unknown but a preponderance of highly functionalized branched and straight-chain lipids of cyanobacterial origin could be one possible cause. Indeed, Kenig (2000) obtained a homologous series of MMAs as pyrolysis products from the kerogen of a Holocene cyanobacteria-dominated mat from an Abu Dhabi sabkha. However, further work needs to be conducted to identify the precise origins of these pyrolysis products.

Regular head-to-tail linked isoprenoids

All samples contain the regular, head-to-tail linked isoprenoids pristane (Pr, *i*-C_{19}) and phytane (Ph, *i*-C_{20}). These isoprenoids are generally regarded as a product of (bacterio)chlorophyll-derived phytol degradation and their ratios are commonly used to interpret redox conditions of ancient depositional environments (e.g., Didyk et al., 1978). Anoxic conditions during diagenesis promote the conversion of phytol to phytane, while oxic conditions promote the conversion to pristane by loss of one terminal carbon atom through decarboxylation (Peters et al., 2005b). Thus, Pr/Ph ratios < 1 are commonly explained by early diagenetic exposure of chlorophyll to reducing conditions, while ratios > 1 suggest elevated oxygen exposure times.

The range of Pr/Ph values in the Gillen samples (0.85 to 1.88; Table 1) suggest that organic matter was exposed to variable redox conditions, possibly by a fluctuating anoxic/oxic boundary within the sediment/water column system. However, the assignment of redox conditions through Pr/Ph is complicated by the existence of other biological sources of regular C_{20} isoprenoids. In hypersaline environments, phytane is often attributed to archaeal core lipids. While phytol in chlorophyll possesses a double bond in β-position of the hydroxyl group that increases its susceptibility to oxidation, the phytanol side-chains of halophilic archaea are fully saturated and less prone to oxidation. Thus, the degradation of these archaeal lipids should yield predominantly phytane, potentially explaining the observation of pure phytane in hypersaline mats (e.g., Jahnke et al., 2008) and the low Pr/Ph ratios (< 1) in most other

568 hypersaline settings (ten Haven et al., 1987). Free phytane has also been identified as a
569 constituent of *Methanococcus* with a variety of dehydrophytenes in other archaeal strains
570 (Tornabene et al., 1979). Thus, redox conditions during the deposition of the Gillen evaporites
571 may have been more oxic than indicated by Pr/Ph, and the large range of values may be
572 influenced by redox variations as well as biological source input.

573 The Gillen samples also contain regular isoprenoids in the carbon number range C_{21} to C_{25}
574 that have a likely haloarchaeal source. Haloarchaea possess three types of membrane lipids
575 with a glycerol backbone that is linked to regular C_{20} and C_{25} isoprenoids via an ether bond: 2,3-
576 di-*O*-phytanyl-*sn*-glycerol (C_{20}, C_{20}-diether); 2-*O*-sesterterpanyl-3-*O*-phytanyl-*sn*-glycerol (C_{25},
577 C_{20}-diether); and 2,3-di-*O*-sesterterpanyl-*sn*-glycerol (C_{25}, C_{25}-diether; e.g., De Rosa et al., 1983;
578 Kates, 1993; Oren, 2002). Some species possess a mixture of these isoprenoids in their
579 membranes with varying proportions of (C_{20}, C_{20}) and (C_{25}, C_{20}) (Oren, 2002). These glycerol
580 diethers are the most likely source of *i*-C_{21} to *i*-C_{25} in the Gillen evaporites.

581 The relative abundance of regular isoprenoids in the Gillen evaporites may hold further
582 information about their origins and environmental specificity. Although *i*-C_{21}, *i*-C_{23} and *i*-C_{24}
583 occur in all samples, *i*-C_{22} was below detection limits. Mass spectra further indicate that *i*-C_{21}, *i*-
584 C_{23} and *i*-C_{24} formed respectively through loss of a butyl, ethyl and methyl group from the tail-
585 end of a regular C_{25} isoprenoid precursor. Cleavage products of the head-end were not
586 observed, and this is also consistent with the absence of *i*-C_{22}, which would form by propyl loss
587 from the head-end of a regular C_{25} isoprenoid precursor. The observation that *i*-C_{21}, *i*-C_{23} and *i*-
588 C_{24} in the Gillen exclusively formed by cleavage of the tail-end, but not the head-end, is
589 important. It indicates that these compounds were generated by diagenetic cleavage of a C_{25}
590 precursor that possessed a functional group at its tail-end, as opposed to later, catagenetic
591 degradation of the unfunctionalized hydrocarbon *i*-C_{25}.

592 A cross-plot of *i*-C_{24}/*i*-C_{25} against Pr/Ph shows a strong positive correlation (R^2 = 0.80; Fig.
593 5A). This correlation demonstrates that the biological precursors of phytane and *i*-C_{25}
594 experienced similar redox conditions during diagenesis and probably had similar functional
595 groups. Thus, we speculate that the bulk of the regular isoprenoids, including pristane and
596 phytane, are derived from (C_{20}, C_{20}), (C_{20}, C_{25}) and (C_{25}, C_{25}) glycerol diethers of Archaea with

597 only a minor contribution from the phytol side chain of (bacterio)chlorophyll. The strong
598 correlation of *i*-C_{24}/*i*-C_{25} and Pr/Ph values also attest to significant oxygen exposure of this
599 archaeal biomass.
600 In samples where acyclic isoprenoids could be isotopically measured, homologues from *i*-
601 C_{23} to *i*-C_{25} yielded $\delta^{13}C$ values between -24.5 and -28.1‰, while the C_{37} to C_{39} head-to-head
602 isoprenoids (also from archaea, see further below) ranged from -25.5 to -26.4‰. These values
603 are similar to the average *n*-alkane values of the respective samples (Table 2) indicating limited
604 differences in the carbon isotopic fractionation between bacteria and archaea.
605
606 *2,6,10,15,19-pentamethylicosane (PMI)*
607 PMI was detected in both dolomite and anhydrite-rich Gillen samples. To our knowledge, the
608 oldest reported occurrence of PMI is in hydrocarbon seep carbonates dating to the Late
609 Pennsylvanian (300 Ma; Birgel et al., 2008). The occurrence of PMI in the Gillen extends the
610 biomarker record of this molecule by more than 500 million years. PMI is widely regarded as a
611 diagnostic biomarker for methanogenic archaea and associated with the methane cycle. This
612 compound has been detected in microbial mats, sediments and sedimentary rocks associated
613 with hydrocarbon seepage and gas hydrates (e.g., Elvert et al., 1999; Thiel et al., 2001; Birgel et
614 al., 2008). In these environments, PMI exhibits strong isotopic depletion and is associated with
615 the anaerobic oxidation of methane (AOM) mediated by consortia of methane-oxidizing
616 archaea and sulfate reducing bacteria (e.g., Hinrichs et al., 1999; Boetius et al., 2000; Valentine,
617 2002). However, in the Gillen samples, PMI is not strongly depleted in ^{13}C, and an association
618 with AOM is unlikely.
619 PMI has also been linked to methylotrophic methanogens that are not characterized by an
620 isotopically strongly depleted biomass (Schouten et al., 1997; Summons et al., 1998; Orphan et
621 al., 2008). Jahnke et al. (2008) and Orphan et al. (2008) detected PMI in the surface layer of a
622 hypersaline microbial mat in Baja California and linked it to the methylotrophic methanogen
623 *Methanolobus* (Orphan et al., 2008). Other studies also link PMI with this methanogen
624 (Schouten et al., 1997; Koga & Morii, 2005) and Orphan et al. (2008) suggested that PMI may be

used as an indicator for the presence of methylotrophic methanogenesis in ancient organic-rich sediments. Thus, the ~820 Ma old PMI may originate from methylotrophic methanogens.

In the Gillen evaporites, strong positive correlations were observed between the PMI/i-C_{25} ratio and [squalane] (R^2 = 0.76; Fig. 6C) and between PMI/i-C_{25} and the head-to-head linked irregular *i*-C_{39} isoprenoid (derived from biphytane, discussed below; R^2 = 0.66; not shown). Intriguingly, in Baja California, Jahnke et al. (2008) and Orphan et al. (2008) observed that PMI has a depth distribution similar to squalene. These compounds were abundant in the uppermost layers (2-10 mm) of the microbial mats but were not detected in deeper layers. The biphytane precursor caldarchaeol was also more abundant in the surface layers of these mats and exhibited lower concentrations in deeper layers. While it is not known whether the PMI, squalane and biphytane in the Gillen evaporites are produced by the same organism, their co-occurrence points to at least a common environmental distribution.

2,6,11,15-tetramethylhexadecane (crocetane)

Crocetane can have two major sources; it is either derived from the breakdown of diaromatic carotenoids (e.g., Brocks & Grice, 2010) or from Archaea associated with methane cycling (e.g., Thiel et al., 1999; Pancost et al., 2000). The oldest reported crocetane, from the 1640 Ma Barney Creek Formation (Greenwood & Summons, 2003), is probably a carotenoid breakdown product as the formation contains abundant diaromatic carotenoids as well as their cleavage products (Brocks & Schaeffer, 2008). By contrast, the Gillen evaporates did not yield any saturated or aromatic carotenoids or their breakdown products (cf. Lee & Brocks, 2011). Furthermore, crocetane exhibited distinct correlation patterns with other molecules (described below). Thus, carotenoid degradation is an unlikely source of the Gillen crocetane.

It is probable that crocetane in the Gillen evaporites is associated with methane cycling. Like PMI, crocetane is generally common in ancient and modern hydrocarbon seeps (e.g., Thiel et al., 2001; Birgel et al., 2008) and gas hydrates (Elvert et al., 1999). Although the source organisms remain unknown, Blumenberg et al. (2004) hypothesized that this molecule is associated with methanotrophic ANME-2, which are a phylogenetically distinct group of

anaerobic archaeal methanotrophs. However, in the Gillen, the combined phytane/crocetane peak did not show any ^{13}C-depletion (Table 2), and an AOM source is thus unlikely.

While crocetane is commonly associated with AOM, the molecule has been detected in lower parts (100 mm) of modern hypersaline cyanobacterial mats from Baja California (Jahnke et al., 2008; Orphan et al., 2008). Enrichment studies showed that deeper sections of these mats produced increased CH_4, while gene analyses revealed the presence of diverse archaeal methanogens belonging to the Methanosarcinales (Orphan et al., 2008). In contrast to the crocetane from AOM settings, the hypersaline equivalents did not exhibit any ^{13}C-depletion and DNA-based phylogenetic analyses did not support a link of this molecule with anaerobic archaeal methanotrophs of ANME-2. Based on the phylogenetic relatedness between the ANME-2 and the hypersaline methanogens, Orphan et al. (2008) postulated a methanogenic source for the crocetane in their study. Since crocetane in the Gillen is not substantially depleted in ^{13}C, it may also be related to halophilic archaeal methanotrophs.

In the Gillen evaporites, negative correlations were observed between relative crocetane concentrations and [squalane] (R^2 = 0.82; Fig. 6B) and between crocetane and the head-to-head linked irregular isoprenoid *i*-C_{39} (derived from biphytane, discussed below; R^2 = 0.79; not shown). These correlations show the opposite trend as those observed for PMI (see above; Fig. 6C), indicating that crocetane and PMI were produced under different environmental conditions (discussed further below).

Biphytane and its breakdown products

The acyclic head-to-head linked isoprenoid biphytane (*i*-C_{40}) and various associated breakdown products were detected in most Gillen samples (Fig. 3D). Biphytane is typically regarded as a breakdown product of archaeal glycerol dibiphytanyl glycerol tetraether (GDGT-0, a.k.a caldarchaeol; e.g., Sinninghe Damsté et al., 2002a,b; Peters et al., 2005b). The breakdown of this compound typically forms a pseudo-homologous series of products that consist of a phytane unit (*i*-C_{20}) coupled head-to-head to a lower carbon-number isoprenoid unit in the range *i*-C_{11} to *i*-C_{20}, or a pristane unit (*i*-C_{19}) joined to an isoprenoid in the range of *i*-C_{10} to *i*-C_{19} (Moldowan & Seifert, 1979; Petrov et al., 1990; Stefanova, 2000; Peters et al., 2005b).

Caldarchaeol is typically linked to all major groups of Archaea except halophiles. Decreasing abundances of caldarchaeol in hypersaline settings is attributed to a shift in community composition from marine Crenarchaeota to halophilic Euryarchaeota (Turich & Freeman, 2011). However, several recent studies revealed the unexpected occurrence of caldarchaeol in modern hypersaline settings. For example, biphytane was detected in a cyanobacterially-dominated microbial mat and underlying sediments from a modern hypersaline lagoon in Baja California (Jahnke et al., 2008). The molecule was particularly abundant in the top 17 mm and coincided with uncultured members of the Euryarchaeota group Thermoplasmatales (Jahnke et al., 2008). Huguet et al. (2015) observed an increase in the proportion of caldarchaeol relative to total GDGTs in hypersaline ponds from Grande-Terre, French West Indies, and suggested production of this compound by halophilic archaea. Turich & Freeman (2011) noted that while halophiles could have the biosynthetic capability to produce biphytane, further work is required to elucidate the presence of caldarchaeol in this group of organisms.

In this study, biphytane breakdown products occurred in both dolomite- and anhydrite-rich samples. Strong correlations between the head-to-head [*i*-C_{39}] and regular [*i*-C_{25}] (R^2 = 0.92; Fig. 5C) and [*i*-C_{39}] and [squalane] (R^2 = 0.93) indicate that the organisms producing these compounds thrived under comparable environmental conditions.

C_{40} tetraether isoprenoids are rarely documented in ancient hypersaline systems. McKirdy & Kantsler (1980) published chromatograms that depict the presence of potential C_{30+} acyclic isoprenoids (see McKirdy & Kantsler, 1980, their Figure 11) from a Cambrian-age hypersaline setting in the Officer Basin, South Australia. Wang & Fu (1997) and Wang (1998) detected a head-to-head acyclic isoprenoid in Cambrian, Permian and Triassic marine hypersaline sequences in China. Therefore, the source organisms of biphytane may be common in hypersaline ecosystems and their discovery in the Gillen Formation pushes the antiquity of these molecules to at least ~820 Ma.

Squalane

Squalane was detected in all Gillen samples and was particularly prominent in anhydrite-rich samples (Fig. 4C). Furthermore, the strong positive correlation of [squalane] with [*i*-C_{25}] (R^2 =

0.93, Fig. 5B) indicates that the source organisms of both molecules thrived under increasing saline conditions. Squalane has been reported in numerous biomarker studies on sedimentary deposits that record ancient hypersaline conditions. For example, Mello et al. (1993, 1994) observed high relative concentrations of squalane in Brazilian rock sequences deposited under hypersaline conditions (e.g., marls and calcareous black shales) as opposed to normal (i.e. less saline) marine and lacustrine black shales. Likewise, Grice et al. (1998) detected squalane in the saline anhydrite deposits of the Miocene/Pliocene Sdom Formation (Israel), but it was not reported from the less saline dolostones of the same formation. Similar results were also reported from Cambrian evaporite sequences in the Officer Basin, South Australia (McKirdy & Kantsler, 1980). Squalane has also been documented in relatively high concentrations in European and North American oils derived from source rocks that are interpreted to be deposited under hypersaline conditions (ten Haven et al., 1988). In all these cases, squalane was inferred to derive from halophilic microorganisms.

The most common biogenic precursor of squalane is squalene, which occurs in all domains of life and serves as a biosynthetic intermediate of polycyclic terpenoids and steroids (Peters et al., 2005b). Squalene is also a major lipid produced by methanogenic (Tornabene et al., 1979; Brassell et al., 1981), thermoacidophilic (e.g., Tornabene et al., 1979) and halophilic (e.g., Tornabene et al., 1969; Stiehl et al., 2005) archaea. Outstanding concentrations of squalane are often seen as indicative for the presence of Archaea (Peters et al., 2005b). This archaeal-source interpretation is reasonable for hypersaline environments such as the Gillen Formation. Indeed, Kamekura (1993) reported that squalenes comprise ~36% of the neutral (nonpolar) lipids in halophiles. Jahnke et al. (2008) and Orphan et al. (2008) detected squalene and several dehydrosqualanes in sedimentary core samples of a modern hypersaline cyanobacterial mat and underlying sediments in Baja California. Furthermore, an isolate of *Methanohalophilus* contained abundant squalene together with small amounts of PMI (Jahnke et al., 2008). Thus, squalane in the Gillen is likely derived from halophilic archaea.

Non-detection of hopanes and steranes in the Gillen Formation

In this study, no indigenous hopanes and steranes were detected in the Gillen samples. A number of biotic and abiotic factors could explain the non-detection of these molecules.

Influence of thermal maturity (catagenesis)

Thermal maturation could have resulted in the degradation of hopanes, steranes and aromatic steroids since cyclic saturated hydrocarbons are generally observed to have lower thermal stabilities than their acyclic counterparts (Peters et al., 2005a). Bruisten (2012) showed that hydrothermal activity affected the Gillen Formation section from which the samples in this study originated, preserving only stratigraphic pockets where indigenous biomarkers could be detected. Based on these localized hydrothermal maturation effects, the Gillen samples exhibit a wide maturity range over a short stratigraphic interval from late-stage oil to mid-stage gas generation. However, the eleven samples chosen for the present study are exceptionally well preserved and mostly fall below a vitrinite reflectance of 1.3. These values are clearly still within the preservation range of hopanoids and steroids (e.g., Peters et al., 2005a). Thus thermal destruction is probably not the cause for the non-detection of polycyclic hydrocarbons in the Gillen samples.

Influence of oxic degradation (diagenesis)

In modern coastal sabkha environments, mats develop in the intertidal zone that is frequently exposed to air (e.g., Bontognali et al., 2010). Similar oxidizing conditions may have been at play in the Gillen environment, potentially destroying hopanols and sterols while preserving more recalcitrant lipids (Pawlowksa et al., 2013). Field and laboratory studies on modern marine sediments show differential degradation of biomarkers under extensive oxic degradation conditions (e.g., Harvey & Macko, 1997; Hoefs et al., 2002; Sinninghe Damsté et al., 2002c). These studies indicate higher resistance of alkenones towards degradation than algal sterols (e.g., Harvey & Macko, 1997). Such degradation patterns were also apparent from sediment trap studies (Prahl et al., 2000). Therefore, oxic degradation could be invoked as a valid explanation for the absence of hopanes and steranes in the Gillen samples. However, hopanols and sterols are still among the most degradation resistant compound classes, and their

768 complete removal from otherwise well preserved sedimentary organic matter appears to be
769 uncommon in modern and Phanerozoic hypersaline environments. For example, steranes,
770 hopanes and gammacerane have been detected in gypsum deposited in the Messinian
771 sedimentary basin under prevailing hypersaline conditions (ten Haven et al., 1985) and sterols
772 are a major constituent of gypsum-rich microbial sediments in the modern shallow hypersaline
773 Lake Tyrrell, Australia, despite frequent exposure to air (Jones, 2011). Low relative abundances
774 of hopanes and steranes were also detected in Miocene/Pliocene halite deposits from the
775 Sdom Formation, Israel (Grice et al., 1998). Thus, while removal of hopanols and sterols from
776 Gillen sediments may have occurred through oxic degradation, the complete removal of these
777 compounds by this process is not particularly likely.
778
779 *Absence of hopanoid and steroid producing organisms*
780 Hopanoids, the precursor of hopanes, are widespread in aerobic (e.g., Farrimond et al., 1998;
781 Brocks & Summons, 2004) and less commonly in anaerobic (e.g., Fischer et al., 2005) bacteria.
782 However, not all bacteria produce hopanoids (e.g., Rohmer et al., 1984) and this may be the
783 case in many hypersaline environments where cyanobacterial mats only yield trace amounts of
784 hopanols. Summons et al. (1999), for example, did not detect any 2-methyl-
785 bacteriohopanepolyols (BHPs) and only trace amounts of C_{32} hopanols in hypersaline
786 cyanobacterial mats from Shark Bay, Australia. Similarly, Rontani & Volkman (2005) only
787 detected small amounts of C_{31} and C_{32} hopanols in coastal hypersaline cyanobacterial mats
788 from Camargue, France, while Bühring et al. (2009) only detected traces of BHPs in a
789 hypersaline cyanobacteria-dominated mat from Kiritimati. Therefore, the absence of detectable
790 indigenous hopanes in the Gillen may be primarily related to low abundances of hopanoid
791 producing bacteria. Furthermore, as pointed out by Brocks & Summons (2004), cyanobacterial
792 hopanoids from hypersaline environments are poorly studied and their occurrence and
793 abundance at different salinity levels is unknown.
794 Sterols, the precursors of steranes and aromatic steroids, occur in nearly all eukaryotes and
795 serve as cell membrane modifiers (e.g., Brocks & Summons, 2004). Some anaerobic ciliates
796 replace sterols with the pentacyclic triterpanoid tetrahymanol, the precursor of gammacerane

(ten Haven et al., 1989). While green algae and predatory ciliates and flagellates can be an important ecological component of modern hypersaline settings (e.g., Javor, 1989; Oren, 2002; Heidelberg et al., 2013), steranes, aromatic steroids and gammacerane remained below detection limits in all Gillen samples. This result is corroborated by a lack of eukaryotic fossils in contemporaneous evaporites from the same area (Oehler et al., 1979). Primary absence of detectable eukaryotic remains in the Gillen may have an ecological or an evolutionary explanation. Although eukaryotes could have existed in the Amadeus Basin during deposition of the Gillen Formation, hypersaline conditions may have reduced their ecological importance. Andrade et al. (2015) detected no sterols or other lipids diagnostic of eukaryotes in a brine pool in hypersaline Lake Tyrrell despite previous observation (Heidelberg et al., 2013) of blooms of the green alga *Dunaliella* and the presence of flagellates in this lake at halite saturation levels. Differences in environmental conditions between sites and at certain periods of time can clearly affect eukaryote abundances, and conditions during deposition of the eleven Gillen samples in this study may have been unsuitable for the formation of eukaryotic blooms. Alternatively, the absence of eukaryotic biomarkers and fossils in the Gillen Formation may be an evolutionary signal. The first appearance of hypersaline eukaryotes is currently unknown. Unambiguous fossils of red algae (Rhodophyta) appear by the late-Mesoproterozoic, while their sister clade, the green algae (Chlorophyta), may go back in time to at least the early-Neoproterozoic (Butterfield, 2015). However, there is currently no information when chlorophytes, or any other group of eukaryotes, started to inhabit hypersaline environments. Hypersaline algae, ciliates and flagellates may simply have evolved after 820 Ma ago.

Paleoecological interpretation of the 820 Ma Gillen Formation

Evidence for haloarchaea

The anhydrites of the Gillen Formation contain abundant *i*-C_{14} to *i*-C_{25} and squalane, biomarkers that are likely derived from haloarchaea. Haloarchaea is the non-taxonomic name for members of the class Halobacteria (McGenity & Oren, 2012), a large group within the archaeal phylum Euryarchaeota. Haloarchaea are found ubiquitously in environments that are saturated or nearly saturated with halite (Falb et al., 2008; McGenity & Oren, 2012; Oren,

826 2012). Like other Archaea, haloarchaea possess lipids based on *i*-C_{20} and sometimes *i*-C_{25} bound
827 to glycerol via ether bonds (e.g., De Rosa et al., 1983; Kates, 1993; Oren, 2002). These lipids
828 impart stability at high salinities with varying concentrations of (C_{20}, C_{25}) and (C_{25}, C_{25}) (Patel &
829 Sprott, 2006). The C_{30} isoprenoid squalene, the precursor of squalane, is another molecule that
830 is abundant in haloarchaea and can play a role in membrane packing and organization (e.g.,
831 Gilmore et al., 2013).
832
833 *Ecological shift between bacteria and archaea with increasing salinity*
834 In extreme hypersaline environments, the relative abundance of halophilic bacteria and
835 archaea can shift rapidly (Andrade et al., 2015). In the Gillen evaporites, the abundance of most
836 archaeal isoprenoids increased relative to bacterial *n*-alkyl lipids with the anhydrite content in
837 the sediment (Fig. 2). To quantify this relationship, we normalized the concentration of
838 isoprenoids relative to closely eluting *n*-alkanes using the expression [*i*-C_x] = 2 * *i*-C_x/(*n*-C_y + *n*-
839 C_{y+1}), where *i*-C_x elutes between *n*-C_y and *n*-C_{y+1}. [*i*-C_x] is an estimate for the relative flux of
840 archaeal and bacterial lipids into the sediment. [*i*-C_{25}], [squalane] and [*i*-C_{39}] all markedly
841 increased with the anhydrite content of the sediments (Fig. 4). These relationships clearly
842 indicate that the abundance of archaea relative to bacteria increased during periods of elevated
843 salinity. The x-y plots of [*i*-C_{25}], [squalane] and [*i*-C_{39}] against anhydrite-percent do not yield
844 simple linear relationships but follow a function resembling a hyperbola (Fig. 4A, C, E). Such
845 hyperbolic relationships are typical of two-component mixing systems. The relationships are
846 consistent with a depositional system that fluctuated between carbonate and sulfate
847 precipitation. Based on the fine dolomite and anhydrite laminae in the Gillen evaporites (Fig. 1),
848 the salinity fluctuations may have been seasonal to decadal.
849 To linearize the apparent hyperbolic functions within the defined data range, we plotted [*i*-
850 C_{25}] against the anhydrite/dolomite ratio (rather than weight-% anhydrite), yielding an
851 approximate linear relationship with a high correlation coefficient (R^2 = 0.87; Fig. 4B). Plots of
852 [squalane] and [*i*-C_{39}] against anhydrite/dolomite yielded even better linear correlations
853 ([squalane]: R^2 = 0.96, Fig. 4D; [*i*-C_{39}]: R^2 = 0.97; Fig. 4F). Relationships of this quality between
854 ecological biomarker parameters and sediment composition have, to our knowledge, not been

observed before. They offer the opportunity to extrapolate the mixing curve to pure dolomite and anhydrite to obtain insights into the community composition during periods of carbonate and sulfate precipitation. The curves in Fig. 4 are fitted mixing scenarios using pure anhydrite and dolomite as the two components. Extrapolation of the curve in Fig. 4D, for example, to pure dolomite yields very low relative squalane abundances ([squalane] ≈ 0.01) indicating that the archaeal source organisms did not play a significant role at low salinities. However, these archaea became ecologically one to two orders of magnitude more important during periods of sulfate precipitation ([squalane] ≈ 0.6). Similarly, the relative abundance of archaeal-derived biphytane breakdown products increased two orders of magnitude in the transition from carbonate to sulfate precipitation (Fig. 4E, F), and haloarchaeal *i*-C_{25} increased by a factor of ~20 relative to bacterial *n*-alkyl lipids (Fig. 4A, B).

These quantitative differences between archaea and bacteria in Gillen carbonates and anhydrites (formerly gypsum) mirror ancient Neogene as well as modern evaporitic environments. Thomas et al. (2015), for example, obtained mainly haloarchaeal and almost no bacterial DNA sequences from the gypsum- and halite-rich layers of cored sediments from the Dead Sea Basin. Alternating carbonate/mud laminae, by contrast, revealed a greater input of bacterial DNA (from KB1 candidate division) and a lower abundance of haloarchaea. Archaeal DNA sequences from these laminae were associated largely with the MSBL1 candidate division sequence and only a small percentage with haloarchaea. It should be noted that some archaea do not only become more abundant with increasing salinity, they also adjust their membrane lipid composition to increasing osmotic pressure. Extreme halophilic archaea (with an optimum growth in 2.5-4.2 mol L^{-1} NaCl at 35°C) contain significant concentrations of both (C_{20}, C_{25}) and (C_{25}, C_{25}) glycerol ethers rather than just (C_{20}, C_{20}), which is also common in many non-halophilic archaea (Patel & Sprott, 2006). These observations are in agreement with a rising *i*-C_{25}/Ph ratio in Gillen samples with increasing proportions of anhydrite (R^2 = 0.59; p <0.01; not shown).

Evidence for halophilic phototrophs

Modern cyanobacteria-dominated mats, such as those from the Gavish Sabkha, occur in almost all salinity ranges, beginning at the metahaline range (4-7%) and ending close to the level of potash salts (> 30%; Gerdes et al., 2000). Microfossils and biomarkers confirm the activity of cyanobacteria in the evaporitic environment of the Gillen Formation. Oehler et al. (1979) discovered possible trichomes as well as spheroidal to ellipsoidal bundles of densely interwoven tubules (2-10 µm in diameter) that were interpreted as cyanobacterial sheaths. Similarly, Knoll (1985) described cyanobacterial microfossils from the Bitter Springs Group and older ancient coastal hypersaline settings from the Paleoproterozoic (1.9 Ga) Belcher Supergroup. In this study, biomarkers indicate the likely presence of cyanobacteria through elevated concentrations and depleted carbon isotopic compositions of *n*-C_{17}. These indications for cyanobacteria have been observed in both dolomite- and gypsum-dominated samples, showing that these organisms, like in modern settings, can occupy both types of facies in hypersaline environments. However, with increasing salinity, cyanobacteria apparently became more important relative to other bacteria; suggested by the negative correlations between $\delta^{13}C$(average *n*-alkanes) and anhydrite content as well as between $\delta^{13}C$(*n*-C_{17}*) and anhydrite content (Fig. 7B, C). As there is no biomarker or fossil evidence for eukaryotic algae, cyanobacteria must have been the dominant primary producer in all Gillen environments. The paucity of eukaryotes is a major deviation from modern hypersaline settings where eukaryotes, such as green algae, can be abundant (e.g., Javor, 1989; Oren, 2002; Heidelberg et al., 2013).

Evidence for halophilic methanogens

Methanogens in hypersaline environments are representatives of the archaea that produce methane as a metabolic byproduct under anoxic conditions. In most environments, methanogens are facing competition with sulfate-reducing bacteria for the products of fermentation such as hydrogen and acetate (McGenity, 2010). Nevertheless, methanogens exist under sulfate-rich hypersaline conditions and methanogenesis becomes an important process in sulfate-depleted deeper sediments (e.g., Wilms et al., 2007), in areas with increased hydrogen production (Hoehler et al., 2001; Buckley et al., 2008), and where non-competitive carbon sources are available (e.g., Winfrey & Ward, 1983).

PMI and crocetane have been detected in the Gillen samples and are associated with methane cycling. While PMI is widely regarded as a diagnostic biomarker for methanogenic archaea, the source of crocetane is unknown. Previous work showed that crocetane and PMI in modern hypersaline mats were not derived from the same source. In the hypersaline mats from Baja California, PMI was prevalent in shallow mats while crocetane was more abundant in deeper layers (Orphan et al., 2008). This observation is consistent with the distribution of these biomarkers in Gillen evaporites. The relative abundance of crocetane increases with dolomite content (R^2 = 0.74; Fig. 6A) and shows negative linear correlations with [squalane] and [*i*-C_{39}] (Fig. 6B). Thus, the source organisms of crocetane were prevalent during periods of carbonate precipitation and became less abundant with increasing sulfate levels. Conversely, PMI/*i*-C_{25} shows a positive relationship with [squalane] and [*i*-C_{39}] (Fig. 6C), indicating that PMI producers were abundant during sulfate precipitation but only played a minor role at lower salinities during carbonate formation. Thus, based on modern and ancient data, PMI producing methanogens appear to tolerate high sulfate concentrations and can compete with sulfate reducing bacteria, while crocetane producers may require lower sulfate levels.

Conclusions

This study demonstrates the capacity of evaporites to serve as archives for the biodiversity and ecology of ancient hypersaline settings dating back as far as ~820 Ma. The sedimentary rocks here studied were composed of alternating laminae of dolomitized microbial mats and up to 90% anhydrite. Although organic matter is thermodynamically unstable in the presence of sulfate, the existence of intact molecular fossils in Gillen Formation evaporites with an anhydrite content up to 90% reveals that hydrocarbon biomarkers can be inert against oxidation by sulfate for hundreds of millions of years. This observation opens the possibility to search for biomarkers in yet older sulfate-rich sediments, including those on Mars.

Solvent extracts of carbonate and anhydrite-rich sedimentary rocks of the Gillen Formation contained a predominance of ^{13}C-depleted heptadecane (*n*-C_{17}), highlighting the presence of cyanobacteria under all salinity regimes. Anhydrite-rich evaporites comprised high relative concentrations of the regular head-to-tail linked isoprenoid *i*-C_{25}, the tail-to-tail linked C_{30}

941 isoprenoid squalane, and the head-to-head linked C_{40} isoprenoid biphytane, consistent with a
942 dominance of halophilic archaea. The irregularly-branched C_{25} isoprenoid PMI with a central
943 tail-to-tail link was also prevalent in anhydrite-rich sediments. The presence of PMI, which did
944 not show a marked carbon isotopic depletion, highlights the activity of archaeal methylotrophic
945 methanogens despite extreme sulfate concentrations. In contrast, the irregularly-branched C_{20}
946 isoprenoid crocetane was more common in dolomite-rich sediments under less saline
947 conditions.

948 The abundance of individual isoprenoids, normalized to *n*-alkanes, showed very good
949 correlations with the anhydrite/dolomite ratio of the evaporites. The relationships are
950 consistent with a two component mixing scenario in which halophilic archaea are the dominant
951 organism in periods of elevated salinity and sulfate precipitation, while bacteria dominated
952 during stages of carbonate formation. Based on fine anhydrite and dolomite laminae in the
953 source rocks, the salinity fluctuations may have been seasonal to decadal in scale.

954 The combination of biomarkers in the mid-Neoproterozoic Gillen Formation is
955 conspicuously similar to modern hypersaline cyanobacterial mats (e.g., Jahnke et al., 2008;
956 Orphan et al., 2008), pointing to a community composition that may have remained broadly
957 constant since at least the late Proterozoic. Only algae and other eukaryotes were
958 conspicuously absent from the ancient hypersaline environment. Given the antiquity of the
959 domain Archaea and the deep root of Halobacteria (e.g., Lake & Sinsheimer, 2013), the
960 existence of these organisms in the mid-Neoproterozoic may not be surprising. However, the
961 Gillen biomarkers and their correlations with salinity are currently the only direct evidence that
962 these organisms were in fact a dominant component of hypersaline ecosystems in the deep
963 past.

964

965 *Acknowledgements*

966 We thank Janet Hope (ANU) for laboratory support, Jamie Lankford, Eddie Resiak (Geoscience
967 Australia) and Maxwell Heckenberg (Northern Territory Geological Survey) for access to drill
968 cores and Emmanuelle Grosjean (Geoscience Australia), Michael Moldowan (Stanford
969 University) and Steven Rowland (University of Plymouth) for providing samples or standards

that were needed for compound identification. We also thank two anonymous reviewers for their comments, which helped to improve the manuscript. This work was financially supported by the Australian Research Council (DP0557499, DP0771043 and DP1095247).

Figure 1. (A) Location of the Amadeus Basin within the Centralian Superbasin (adapted with modifications from Logan et al., 1999). Star denotes the location of the *Mt Charlotte 1* core. **(B)** Composite stratigraphic section of the Precambrian / Cambrian time interval in the Amadeus Basin, central Australia (adapted with modifications from Skotnicki et al., 2008). Strata of interest are highlighted in yellow. **(C)** Anhydrite-rich Gillen Formation evaporite (08r022, 1650.8 m). Coins in (C) and (E) are 2.5 cm in diameter. **(D)** Transmitted light micrograph of anhydrite-rich Gillen evaporite exhibiting interspersed bedding of dolomite in thin section (08r022, 1650.8 m). Scale bar represents 1.5 cm. **(E)** Gillen evaporite showing alternating laminae of dolomite (dark layers) and anhydrite (light layers; 08r009, 1654.5 m). **(F-G)** Transmitted light micrographs of Gillen evaporites exhibiting alternate laminae of dolomite (dark brown layers) and anhydrite (colourless layers; (F) from 08r008, 1654 m; (G) from 08r009, 1654.5 m). Scale bar in (F) represents 1.5 cm, and in (G) 100 µm. **(H)** Reflected light micrograph of a dark dolomitic layer revealing dolomite crystals interlayered with dark fibrous clay-rich laminae (08r008; 1654 m). Scale bar represents 100 µm.

Figure 2. Total ion chromatograms (TIC) of representative saturate fractions from Gillen Formation evaporites composed of **(A)** predominantly dolomite (77%; 08r006; 1655 m depth), **(B)** a mixture of anhydrite (76.8%) and dolomite (15%; 08r008; 1654 m depth), and **(C)** predominantly anhydrite (90%; 08r022; 1650.8 m depth). Small solid black spheres = *n*-alkanes; large solid black spheres = monomethylalkanes; large empty spheres = dimethylalkanes; red triangles = regular head-to-tail linked isoprenoids; blue triangles = irregular tail-to-tail linked isoprenoid 2,6,10,15,19-pentamethylicosane (PMI); brown triangles = irregular tail-to-tail linked isoprenoid 2,6,11,15-tetramethylhexadecane (crocetane); green triangles = irregular head-to-

head linked isoprenoids; yellow triangle = irregular tail-to-tail isoprenoid (squalane); X = unidentified acyclic isoprenoids; IS = internal standard; UCM = unresolved complex mixture.

Figure 3. (A) Partial *m/z* 183 mass chromatogram showing the distribution of head-to-tail linked isoprenoids (with carbon numbers) in a Gillen Formation evaporite (08r022; 1650.8 m depth). Pr = pristane; Ph = phytane; X = unidentified acyclic isoprenoids. Unlabeled peaks are largely *n*-alkanes and monomethylalkanes. This sample represents a silicalite non-adduct. **(B)** Partial mass chromatograms showing a comparison of the elution position of i) crocetane from Gillen evaporite (09r001; 1652 m depth) at *m/z* 169 with ii) the subtraction of ions *m/z* 169-197 in the same Gillen sample, and iii) a co-injected mix of pure crocetane and the same sample as above. X = unknown acyclic isoprenoid. **(C)** Partial *m/z* 183 mass chromatograms indicating the presence of 2,6,10,15,19-pentamethylicosane (PMI) in Gillen evaporite (08r008; 1654 m depth). i) PMI from a New Zealand hydrocarbon seep carbonate. ii) PMI elution region in the Gillen sample, showing a peak at the same position as in i). Note that the Gillen PMI peak co-elutes with regular *i*-C_{25}. X = unknown acyclic isoprenoid **(D)** Partial *m/z* 183 mass chromatogram showing the distribution of head-to-head isoprenoids in i) Miocene crude oil from California and ii) in a Gillen evaporite (08r008; 1654 m depth). Unlabeled peaks are *n*-alkanes and regular isoprenoids.

Figure 4. Biomarker / mineral relationships. **(A)** Regular [*i*-C_{25}] vs. anhydrite (weight %). **(B)** Regular [*i*-C_{25}] vs. anhydrite/dolomite (weight/weight ratio). **(C)** [squalane] vs. anhydrite. **(D)** [squalane] vs. anhydrite/dolomite. **(E)** [*i*-C_{39}] vs. anhydrite. **(F)** [*i*-C_{39}] vs. anhydrite/dolomite. [Z] is the concentration of compound Z relative to nearby eluting n-alkanes (see text).

Figure 5. Isoprenoid biomarker relationships. **(A)** Pristane/phytane vs. regular *i*-C_{24}/*i*-C_{25} ratios. **(B)** [squalane] vs. regular [*i*-C_{25}]. **(C)** Irregular [*i*-C_{39}] vs. regular [*i*-C_{25}]. [Z] is the concentration of compound Z relative to nearby eluting n-alkanes (see text).

Figure 6. Isoprenoids from methanogens and their mineral and biomarker relationships. **(A)** Crocetane/phytane vs. dolomite (weight %). **(B)** Crocetane/phytane vs. [squalane]. **(C)** PMI/ *i*-C_{25} vs. [squalane].

Figure 7. Compound specific $\delta^{13}C$ values and mineral relationships. Isotope values for individual samples and compounds are presented in Table 2. **(A)** $\delta^{13}C$ values of *n*-alkanes plotted against chain length. Values for *n*-C_{24} are not included due to co-elution with 18-methyleicosanoic acid methyl ester internal standard. **(B)** Average $\delta^{13}C$ values of *n*-alkanes vs. anhydrite (weight %). **(C)** Excess isotopic depletion of *n*-C_{17} ($\delta^{13}C$(*n*-C_{17}*)) vs. anhydrite. $\delta^{13}C$(*n*-C_{17}*) = $\delta^{13}C$(*n*-C_{17}) – ($\delta^{13}C$(*n*-C_{16}) + $\delta^{13}C$(*n*-C_{18}))/2.

Table 1. Mineralogical, bulk organic geochemical, textural and thermal maturity characteristics of Neoproterozoic Gillen Formation samples from *Mt Charlotte 1.*

Table 1 footnotes

Compound abbreviations: Pr = pristane; ph = phytane; MA = methyladamantane; MD = methyldiamantane; Phen = phenanthrene; MP = methylphenanthrene; MDBT = methyldibenzothiophene; DMDBT = dimethyldibenzothiophene; TMN = trimethylnaphthalene; MN = methylnaphthalene. Maturity compound ratio abbreviations and definitions: MAI = methyladamantane index (1-MA/[1-MA + 2-MA]); MDI = methyldiamantane index (4-MD/[1-MD + 3-MD + 4-MD]); MPI-1 = methylphenanthrene index (1.5 x [3-MP + 2-MP]/[Phen + 9-MP + 1-MP]); MPR = methylphenanthrene ratio (2-MP/1-MP); MPDF = methylphenanthrene distribution factor ([3-MP + 2-MP]/[3-MP + 2-MP + 9-MP + 1-MP]); MDR = methyldibenzothiophene ratio (4-MDBT/1-MDBT); DMDR = dimethyldibenzothiophene ratio (4,6-DMDBT/[3,6- + 2,6-DMDBT]); TNR-1 = trimethylnaphthalene ratio (2,3,6-TMN/[1,4,6- +

1,3,5-TMN]); TNR-2 = trimethylnaphthalene ratio (2,3,6- + 1,3,7-TMN/[1,4,6- + 1,3,5- + 1,3,6-TMN]); MNR = methylnaphthalene ratio (2-MN/1-MN). n.d. = not determined; Sat = saturates; Aro = aromatics. *a* = mineral quantities (in weight %) measured using XRPD and Siroquant V3. Only percentages of anhydrite and dolomite are shown – remaining minerals are combinations of quartz, feldspar, clay, pyrite and halite. *b* = Organic carbon content of pre-extracted samples (weight %). *c* = Ratio calculated on partial (*m/z* 268 and 282) molecular ion chromatograms to minimize interference from co-eluting compounds; resulting values where divided by a correction factor of 1.2 to account for differences in response. *d* = expressed in ppm (relative to mass of extracted rock).

Table 2. Carbon stable isotope data of Neoproterozoic Gillen Formation samples from *Mt Charlotte 1*

Table 2 footnotes

Abbreviations: Pr = pristane; Ph+Croc = combined phytane and crocetane isotopic signal; *i*-C_{25}+PMI = combined regular C_{25} isoprenoid and PMI isotopic signal; *i*-C_{21} to *i*-C_{25} = regular, head-to-tail linked isoprenoids; *i*-C_{37} to *i*-C_{39} = irregular, head-to-head linked isoprenoids; n.d. = not determined. *a* = average $\delta^{13}C$ of all *n*-alkanes in a sample. *b* = Isotopic depletion of *n*-C_{17} relative to nearby eluting *n*-alkanes $\delta^{13}C(n\text{-}C_{17}^{*}) = \delta^{13}C(n\text{-}C_{17}) - (\delta^{13}C(n\text{-}C_{16}) + \delta^{13}C(n\text{-}C_{18}))/2$.

REFERENCES

Alexander, R., Bastow, T.P., Fisher, S.J., & Kagi R.I. (1995). Geosynthesis of organic compounds: II. Methylation of phenantherene and alkylphenanthrenes. *Geochimica et Cosmochimica Acta*, 59, 4259-4266.

Alexander, R., Berwick, L., & Pierce, K. (2011). Single carbon surface reactions of 1-octadecene and 2,3,6-trimethylphenol on activated carbon: Implications for methane formation in sediments. *Organic Geochemistry*, 42, 540-547.

Alexander, R., Kagi, R., Rowland, S.J., Sheppard, P.N., & Chirila, T.V. (1985). The effects of thermal maturity on distributions of dimethylnaphthalenes and trimethylnaphthalenes in some Ancient sediments and petroleums. *Geochimica et Cosmochimica Acta*, 49, 385-395.

Andrade, K., Logemann, J., Heidelberg, K.B., Emerson. J.B., Comolli, L.R., Hug, L.A., Probst, A.J., Keillar, A., Thomas, B.C., Miller, C.S., Allen, E.E., Moreau, J.W., Brocks, J.J., & Banfield J.F. (2015). Metagenomic and lipid analyses reveal a diel cycle in a hypersaline microbial ecosystem. *The ISME Journal*, 9, 2697-2711.

Birgel, D., Himmler, T., Freiwald, A., & Peckmann, J. (2008). A new constraint on the antiquity of anaerobic oxidation of methane: Late Pennsylvanian seep limestones from southern Namibia. *Geology*, 36, 543-546.

Blumenberg, M., Seifert, R., Reitner, J., Pape, T., & Michaelis, W. (2004). Membrane lipid patterns typify distinct anaerobic methanotrophic consortia. *Proceedings of the National Academy of Sciences*, 101, 11111-11116.

Boetius, A., Ravenschlag, K., Schubert, C.J., Rickert, D., Widdel, F., Gieseke, A., Amann, R., Jørgensen, B.B., Witte, U., & Pfannkuche, O. (2000). A marine consortium apparently mediating anaerobic oxidation of methane. *Nature*, 407, 623-626.

Bontognali, T.R.R., Vasconcelos, C., Warthmann, R.J., Bernasconi, S.M., Dupraz, C., Strohmenger, C.J., & McKenzie, J.A. (2010). Dolomite formation within microbial mats in the coastal sabkha of Abu Dhabi (United Arab Emirates). *Sedimentology*, 57, 824-844.

Boreham, C.J., Crick, I.H., & Powell, T.G. (1988). Alternative calibration of the methylphenanthrene index against vitrinite reflectance: Application to maturity measurements on oils and sediments. *Organic Geochemistry*, 12, 289-294.

Brassell, S.C., Wardroper, A.M.K., Thompson, I.D., Maxwell, J.R., & Eglington, G. (1981). Specific acyclic isoprenoids as biological markers of methanogenic bacteria in marine sediments. *Nature*, 290, 693-696.

Brocks, J.J. (2011). Millimeter-scale concentration gradients of hydrocarbons in Archean shales: Live-oil escape or fingerprint of contamination? *Geochimica et Cosmochimica Acta*, 75, 3196-3213.

Brocks, J.J., Buick, R., Logan, G.A., & Summons, R.E. (2003a). Composition and syngeneity of molecular fossils from the 2.78 to 2.45 billion-year-old Mount Bruce Supergroup, Pilbara Craton, Western Australia. *Geochimica et Cosmochimica Acta,* 67, 4289-4319.

Brocks, J.J., Buick, R., Summons, R.E., & Logan, G.A. (2003b). A reconstruction of Archean biological diversity based on molecular fossils from the 2.78 to 2.45 billion-year-old Mount Bruce Supergroup, Hamersley Basin, Western Australia. *Geochimica et Cosmochimica Acta*, 67, 4321-4335.

Brocks, J.J., & Grice, K. (2010). Biomarkers (Molecular Fossils). In: *Encyclopaedia of Biogeology* (eds Thiel V, Reitner J). Springer, pp. 36.

Brocks, J.J., Grosjean, E., & Logan, G.A. (2008). Assessing biomarker syngeneity using branched alkanes with quaternary carbon (BAQCs) and other plastic contaminants. *Geochimica et Cosmochimica Acta*, 72, 871-888.

Brocks, J.J., & Hope, J.M. (2014). Tailing of chromatographic peaks in GC‐MS caused by interaction of halogenated solvents with the ion source. *Journal of Chromatographic Sciences*, 52, 471-475.

Brocks, J.J., & Schaeffer, P. (2008). Okenane, a biomarker for purple sulphur bacteria (Chromatiaceae), and other new carotenoid derivatives from the 1640 Ma Barney Creek Formation. *Geochimica et Cosmochimica Acta*, 72, 1396-1414.

Brocks, J.J., & Summons, R.E. (2004). Sedimentary hydrocarbons, biomarkers for early life. In: *Treaties on Geochemistry – Biogeochemistry* 8, (eds Holland HD, Turekian KK). Elsevier, pp. 63-115.

Bruisten, B. (2012). *Preservation and destruction of biomarkers in Neoproterozoic evaporites of the 800 Ma Bitter Springs Formation, Amadeus Basin, Central Australia*. Master Thesis, RWTH Aachen University.

Buckley, D.H., Baumgartner, L.K., & Visscher, P.T. (2008). Vertical distribution of methane metabolism in microbial mats of the Great Sippewissett Salt Marsh. *Environmental Microbiology*, 10, 967-977.

Bühring, S.I., Smittenberg, R.H., Sachse, D., Lipp, J.S., Golubic, S., Sachs, J.P., Hinrichs, K.-U., & Summons, R.E. (2009). A hypersaline microbial mat from the Pacific Atoll Kiritimati: Insights into composition and carbon fixation using biomarker analyses and a ^{13}C-labeling approach. *Geobiology*, 7, 308-323.

Butterfield, N.J. (2015). Early evolution of the Eukaryota. Palaeontology, 58, 5-17.

Chen, J., Fu, J., Sheng, G., Liu, D., & Zhang, J. (1996). Diamondoid hydrocarbon ratios: Novel maturity indices for highly mature crude oils. *Organic Geochemistry*, 25, 179-190.

De Rosa, M., Gambacorta, A., Nicolaus, B., & Grant, W.D. (1983). A C_{25}, C_{25} diether core lipid from archaebacterial haloalkaliphiles. *Journal of General Microbiology*, 129, 2333-2337.

Des Marais D.J., Cohen Y., Nguyen H., Cheatham M., Cheatham T., & Munoz E. (1989). Carbon isotopic trends in the hypersaline ponds and microbial mats at Guerrero Negro, Baja California Sur, Mexico: Implications for Precambrian stromatolites. In: *Microbial Mats: Physiological Ecology of Benthic Microbial Communities* (eds Cohen Y., Rosenberg E.) American Society for Microbiology, Washington, pp. 191-203.

Didyk, B.M., Simoneit, B.R.T., Brassell, S.C., & Eglington, G. (1978). Organic geochemical indicators of palaeoenvironmental conditions of sedimentation. *Nature*, 272, 216-222.

1173 Dow, W.G. (1977). Kerogen studies and geological interpretations. *Journal of Geochemical*
1174 *Exploration*, 7, 79-99.
1175
1176 Edgoose, C.J. (2012). The Amadeus Basin, central Australia. *Episodes*, 35, 256-263.
1177
1178 Elvert, M., Suess, E., & Whiticar, M.J. (1999). Anaerobic methane oxidation associated with marine
1179 gas hydrates: Superlight C-isotopes from saturated and unsaturated C_{20} and C_{25} irregular
1180 isoprenoids. *Naturwissenschaften*, 86, 295-300.
1181
1182 Espitalie, J., Madec, M., & Tissot, B. (1980). Role of mineral matrix in kerogen pyrolysis: Influence on
1183 petroleum generation and migration. *AAPG Bulletin*, 64, 59-66.
1184
1185 Falb, M., Müller, K., Königsmaier, L., Oberwinkler, T., Horn, P., von Gronau, S., Gonzalez, O., Pfeiffer,
1186 F., Bornberg-Bauer, E., & Oesterhelt, D. (2008). Metabolism of halophilic archaea. *Extremophiles*,
1187 12, 177-196.
1188
1189 Farrimond, P., Fox, P.A., Innes, H.E., Miskin, I.P., & Head, I.M. (1998). Bacterial sources of hopanoids
1190 in recent sediments: Improving our understanding of ancient hopanes biomarkers. *Ancient*
1191 *Biomolecules,* 2, 147-166.
1192
1193 Fischer, W.W., Summons, R.E., & Pearson, A. (2005). Targeted genomic detection of biosynthetic
1194 pathways: Anaerobic production of hopanoid biomarkers by a common sedimentary microbe.
1195 *Geobiology*, 3, 33-40.
1196
1197 Fowler, M.G., Abolins, P., & Douglas, A.G. (1986). Monocyclic alkanes in Ordovician organic matter.
1198 *Organic Geochemistry*, 10, 815-823.
1199
1200 Fowler, M.G., & Douglas, A.G. (1987). Saturated hydrocarbon biomarkers in oils of Late Precambrian
1201 age from eastern Siberia. *Organic Geochemistry*, 11, 201-213.
1202

García-Maldonado, J.Q., Bebout, B.M., Everroad, R.C., & López-Cortés, A. (2015). Evidence for novel phylogenetic lineages of methanogenic Archaea from hypersaline microbial mats. *Microbial Ecology*, 69, 106-117.

Gelin, F., De Leeuw, J.W., Sinninghe Damsté, J.S., Derenne, S., Largeau, C., & Metzger, P. (1994). The similarity of chemical structures of soluble aliphatic polyaldehyde and insoluble algaenan in the green microalga *Botryococcus braunii* race A as revealed by analytical pyrolysis. Organic Geochemistry, v. 21, p. 423-435.

Gerdes, G., Krumbein, W.E., & Noffke, N. (2000). Evaporite microbial sediments. In: *Microbial Sediments* (eds Riding RE, Awramik SM). Springer, pp. 196-208.

Gilmore, S.F., Yao, A.I., Tietel, Z., Kind, T., Facciotti, M.T., & Parikh, A.N. (2013). Role of squalene in the organization of monolayers derived from lipid extracts of *Halobacterium salinarum*. *Langmuir*, 29, 7922-7930.

Greenwood, P.F., & Summons, R.E. (2003). GC-MS detection and significance of crocetane and pentamethylicosane in sediments and crude oils. *Organic Geochemistry*, 34, 1211-1222.

Grice, K., Schouten, S., Nissenbaum, A., Charrach, J., & Sinninghe Damstè, J.S. (1998). Isotopically heavy carbon in the C_{21} to C_{25} regular isoprenoids in halite-rich deposits from the Sdom Formation, Dead Sea Basin, Israel. *Organic Geochemistry*, 28, 349-359.

Grimalt, J.O., De Wit, R., Teixidor, P., & Albaiges, J. (1992). Lipid biogeochemistry of *Phormidium* and *Microcoleus* mats. *Organic Geochemistry*, 19, 509-530.

Halverson, G.P., Dudás, F.Ö., Maloof, A.C., & Bowring, S.A. (2007). Evolution of the $^{87}Sr/^{86}Sr$ composition of Neoproterozoic seawater. *Palaeogeography, Palaeoclimatology, Palaeoecology*, 256, 103-129.

Han, J., McCarthy, E.D., Calvin, M., & Benn, M.H. (1968). Hydrocarbon constituents of the blue-green algae *Nostoc muscurum, Anacystis nidulans, Phormidium luridum* and *Chlorogloea fritschii*. *Journal of the Chemical Society C*, 22**,** 2785-2791.

Harvey, H.R., & Macko, S.A. (1997). Catalysts or contributors? Tracking bacterial mediation of early diagenesis in the marine water column. *Organic Geochemistry*, 26, 531-544.

Heidelberg, K.B., Nelson, W.C., Holm, J.B., Eisenkolb, N., Andrade, K., & Emerson, J.B. (2013). Characterization of eukaryotic microbial diversity in hypersaline Lake Tyrrell, Australia. *Frontiers in Microbiology*, 4, 115.

Hill, A.C., Arouri, K., Gorjan, P., & Walter, M.R. (2000). Geochemistry of marine and non-marine environments of a Neoproterozoic cratonic carbonate/evaporite: The Bitter Springs Formation, Central Australia. In: *Carbonate Sedimentation and Diagenesis in an Evolving Precambrian World* (eds Grotzinger JP, James NP). SEPM Special Publication, 67, pp. 327-344.

Hinrichs, K.-U., Hayes, J.M., Sylva, S.P., Brewer, P.G., & DeLong, E.F. (1999). Methane-consuming archaebacteria in marine sediments. *Nature*, 398, 802-805.

Hoefs, M.J.L., Rijpstra, W.I.C., & Sinninghe Damsté, J.S. (2002). The influence of oxic degradation on the sedimentary biomarker record I: Evidence from Madeira Abyssal Plain turbidites. *Geochimica et Cosmochimica Acta*, 66, 2719-2735.

Hoehler, T.M., Bebout, B.M., & Des Marais, D.J. (2001). The role of microbial mats in the production of reduced gases on the early Earth. *Nature*, 412, 324-327.

Hoering, T.C. (1981). Monomethyl, acyclic hydrocarbons in petroleum and source extracts. *Carnegie Institute of Washington Yearbook*, 80, 389-394.

Hoffmann, C.F., Foster, C.B., Powell, T.G., & Summons, R.E. (1987). Hydrocarbon biomarkers from Ordovician sediments and the fossil alga *Gloeocapsomorpha prisca* Zalessky 1917. *Geochimica et Cosmochimica Acta*, 51, 2681-2697.

Hoffman, P.F., Kaufman, A.J., Halverson, G.P., & Schrag, D.P. (1998). A Neoproterozoic snowball Earth. *Science*, 281, 1342-1346.

Holland, H.D. (1984). *The Chemical Evolution of the Atmosphere and Oceans*. Princeton University Press.

House, C.H., Schopf, J.W., McKeegan, K.D., Coath, C.D, Harrison, T.M., & Stetter, K.O. (2000). Carbon isotopic composition of individual Precambrian microfossils. *Geology*, 28, 707-710.

Huguet, A., Grossi, V., Belmahdi, I., Fosse, C., & Derenne, S. (2015). Archaeal and bacterial tetraether lipids in tropical ponds with contrasting salinity (Guadeloupe, French West Indies): Implications for tetraether-based environmental proxies. *Organic Geochemistry*, 83-84, 158-169.

Javor, B.J. (1989). *Hypersaline Environments: Microbiology and Biogeochemistry*. Brock/Springer Series, Berlin, Heidelberg, New York.

Jahnke, L.L., Orphan, V.J., Embaye, T., Turk, K.A., Kubo, M.D., Summons, R.E., & Des Marais, D.J. (2008). Lipid biomarker and phylogenetic analyses to reveal archaeal biodiversity and distribution in hypersaline microbial mat and underlying sediment. *Geobiology*, 6, 394-410.

Jarrett, A.J.M., Schinteie, R., & Brocks, J.J. (2013). Micro-ablation, a new technique to remove drilling fluids and other contaminants from fragmented and fissile rock material. *Organic Geochemistry*, 61, 57-65.

Jones, C.M. (2011). *Reconstruction of microbial and environmental conditions in an Australian hypersaline ecosystem from the mid-Pleistocene through the present*. PhD thesis, University of California, Berkeley.

Kamekura, M. (1993). Lipids of extreme halophiles. In: *The Biology of Halophilic Bacteria* (eds Vreeland RH, Hochstein LI). CRC Press, Boca Raton, Florida, pp. 135-161.

Kates, M. (1993). Membrane lipids of extreme halophiles: Biosynthesis, function and evolutionary significance. *Experientia*, 49, 1027-1036.

Katz, B.J. (1983). Limitations of Rock-Eval pyrolysis for typing organic matter. *Organic Geochemistry,* 4, 195-199.

Kenig, F. (2000). C_{16}-C_{29} homologous series of monomethylalkanes in the pyrolysis products of a Holocene microbial mat. *Organic Geochemistry*, 31, 237-241.

Kenig, F., Sinninghe Damsté, J.S., Kock-van Dalen, A.C., Rijpstra, W.I.C., Huc, A.Y., & de Leeuw, J.W. (1995). Occurrence and origin of mono-, di, and trimethylalkanes in modern and Holocene cyanobacterial mats from Abu Dhabi, United Arab Emirates. *Geochimica et Cosmochimica Acta*, 59, 2999-3015.

Kissin, Y.V. (1987) Catagenesis and composition of petroleum: Origin of *n*-alkanes and isoalkanes in petroleum crudes. *Geochimica et Cosmochimica Acta*, 51, 2445-2457.

Klaebe, R.M., Kennedy, M.J., Jarrett, A.J.M., & Brocks, J.J. (2016). Local paleoenvironmental controls on the carbon-isotope record defining the Bitter Springs Anomaly. *Geobiology*, 15, 65-85.

Klomp, U.C. (1986). The chemical structure of a pronounced series of iso-alkanes in South Oman crudes. *Organic Geochemistry*, 10, 807-814.

Knoll, A.H. (1985). A paleobiological perspective on Sabkhas. In: *Hypersaline Ecosystems: The Gavish Sabkha* (eds Friedman GM, Krumbein WE), Springer-Verlag, Berlin, pp. 407–425.

Koga, Y., & Morii, H. (2005). Recent advances in structural research on ether lipids from archaea including comparative and physiological aspects. *Bioscience, Biotechnology and Biochemistry*, 69, 2019-2034.

Kristen, I., Wilkes, H., Vieth, A., Zink, K.-G., Plessen, B., Thorpe, J., Partridge, T.C., & Oberhänsli, H. (2010). Biomarker and stable carbon isotope analyses of sedimentary organic matter from Lake Tswaing: evidence for deglacial wetness and early Holocene drought from South Africa. *Journal of Paleolimnology*, 44, 143-160.

Kvalheim, O.M., Christy, A.A., Telnæs, N., & Bjørseth, A. (1987). Maturity determination of organic matter in coals using the methylphenanthrene distribution. *Geochimica et Cosmochimica Acta*, 51, 1883-1888.

Lake, J.A., & Sinsheimer, J.S. (2013). The deep roots of the rings of life. *Genome Biology and Evolution*, 8, 2440-2448.

Lee, C., & Brocks, J.J. (2011). Identification of carotane breakdown products in the 1.64 billion year old Barney Creek Formation, McArthur Basin, northern Australia. *Organic Geochemistry*, 42, 425-430.

Lindsay, J.F. (1987). Upper Proterozoic evaporites in the Amadeus Basin, central Australia, and their role in basin tectonics. *Geological Society of America Bulletin*, 99, 852-865.

Logan, G.A., Calver, C.R., Gorjan, P., Summons, R.E., Hayes, J.M., & Walter, M.R. (1999). Terminal Proterozoic mid-shelf benthic microbial mats in the Centralian Superbasin and their environmental significance. *Geochimica et Cosmochimica Acta*, 63, 1345-1358.

Logan, G.A., Hayes, J.M., Hieshima, G.B., & Summons, R.E. (1995). Terminal Proterozoic reorganization of biogeochemical cycles. *Nature*, 376, 53–56.

Logan, G.A., Summons, R.E., & Hayes, J.M. (1997). An isotopic biogeochemical study of Neoproterozoic and Early Cambrian sediments from the Centralian Superbasin, Australia. *Geochimica et Cosmochimica Acta*, 61, 5391-5409.

McGenity, T.J. (2010). Methanogens and methanogenesis in hypersaline environments. In: *Handbook of Hydrocarbon and Lipid Microbiology* (ed Timmis KN), Springer-Verlag, Berlin, Heidelberg, pp. 665-680.

McGenity, T.J., & Oren, A. (2012). Life in saline environments. In: *Life at Extremes. Environments, Organisms, and Strategies for Survival* (ed Bell EM). CABI International, Wallingford, UK, pp. 402–437.

McKirdy, D.M., & Kantsler, A.J. (1980). Oil geochemistry and potential source rocks of the Officer Basin, South Australia. *APEA Journal*, 20, 68-86.

McTaggart, N.R., Pemberton, R.L., & Planalp, R.N. (1965). *Well Completion Report. Mount Charlotte No. 1*. Transoil (N.T.) Pty.

Mello, M.R., Koutsoukos, E.A.M., Santos Neto, E.V., & Silva Telles, A.C. Jr. (1993). Geochemical and micropaleontological characterization of lacustrine and marine hypersaline environments from Brazilian sedimentary basins. In: *Source Rocks in a Sequence Stratigraphic Framework* (eds Katz BJ, Pratt LM). American Association of Petroleum Geologists, Tulas, OK, pp. 17-34.

Mello, M.R., Koutsoukos, E.A.M., Mohriak, W.U., & Bacoccoli, G. (1994). *Selected petroleum systems in Brazil. In: The Petroleum System – From Source to Trap* (eds Magoon LB, Dow WG). American Association of Petroleum Geologists, Tulsa, OK, pp. 499-512.

Moldowan, J.M., & Seifert, W.K. (1979). Head-to-head linked isoprenoid hydrocarbons in petroleum. *Science*, 204, 169-171.

Oehler, D.Z., Oehler, J.H., & Stewart, A.J. (1979). Algal fossils from a late Precambrian, hypersaline lagoon. *Science*, 205, 388-390.

Oren, A. (2002). *Halophilic Microorganisms and their Environments.* Kluwer Academic, Springer, Dordrecht.

Oren, A. (2012). Taxonomy of the family *Halobacteriaceae*: A paradigm for changing concepts in prokaryote systematics. *International Journal of Systematic and Evolutionary Microbiology*, 62, 263-271.

Orphan, V.J., Jahnke, L.L., Embaye, T., Turk, K.A., Pernthaler, A., Summons, R.E., & Des Marais, D.J. (2008), Characterization and spatial distribution of methanogens and methanogenic biosignatures in hypersaline microbial mats of Baja California. *Geobiology*, 6, 376-393.

Pancost, J.S., Sinninghe Damsté, J.S., de Lint, S., van der Maarel, M.J.E.C., & Gottschal, J.C. (2000). Biomarker evidence for widespread anaerobic methane oxidation in Mediterranean sediments by a consortium of methanogenic archaea and bacteria. *Applied and Environmental Microbiology*, 67, 1126–1132.

Patel, G.B., & Sprott, G.D. (2006). Archaeal Membrane Lipids. In: *Encyclopedia of Life Sciences*. Nature Publishing Group, London, doi: 10.1038/npg.els.0004316.

Pawlowska, M.M., Butterfield, N.J., & Brocks, J.J. (2013). Lipid taphonomy in the Proterozoic and the effect of microbial mats on biomarker preservation. *Geology*, 41, 103-106.

Peters, K.E., Walter, C.C., & Moldowan, M.J. (2005a). *The Biomarker Guide: Biomarkers and Isotopes in the Environments and Human History*. 2nd edition, volume 1, New York, Cambridge University Press.

Peters, K.E., Walters, C.C., & Moldowan, M.J. (2005b). *The Biomarker Guide: Biomarkers and Isotopes in Petroleum Exploration and Earth History*. 2nd edition, volume 2, New York, Cambridge University Press.

Petrov, A.A., Vorobyova, N.S., & Zemskova, Z.K. (1990). Isoprenoid alkanes with irregular "head-to-head" linkages. *Organic Geochemistry*, 16, 1001-1005.

Prahl, F.G., Dymond, J., & Sparrow, M.A. (2000). Annual biomarker record for export production in the central Arabian Sea. *Deep-Sea Research*, 47, 1581-1604.

Radke, M., Welte, D.H., & Willsch, H. (1982a). Geochemical study on a well in the western Canada Basin: relation of the aromatic distribution pattern to maturity of organic matter. *Geochimica et Cosmochimica Acta*, 46, 1-10.

Radke, M., Welte, D.H., & Willsch, H. (1986). Maturity parameters based on aromatic hydrocarbons: Influence of the organic matter type. *Organic Geochemistry*, 10, 51-63.

Radke, M., Willsch, H., Leythaeuser, D., & Teichmüller, M. (1982b). Aromatic compounds of coal; relation of distribution pattern to rank. *Geochimica et Cosmochimica Acta*, 46, 1831-1848.

Řezanka, T., Zahradník, J., & Podojil, M. (1982). Hydrocarbons in green and blue-green algae. *Folia Microbiologica*, 27, 450-454.

Risatti, J.B., Rowland, S.J., Yon, D.A., & Maxwell, J.R. (1984). Stereochemical studies of acyclic isoprenoids – XII. Lipids of methanogenic bacteria and possible contributions to sediments. *Organic Geochemistry*, 6, 93–104.

Robson, J.N. (1987). *Synthetic and biodegradation studies of some sedimentary isoprenoid hydrocarbons*. PhD Thesis, Plymouth Polytechnic.

Robson, J.N., & Rowland, S.J. (1993). Synthesis, chromatographic and spectral characterisation of 2,6,11,15-tetramethylhexadecane (crocetane) and 2,6,9,13-tetramethyltetradecane: reference acyclic isoprenoids for geochemical studies. *Organic Geochemistry*, 20, 1093-1098.

Rohmer, M., Bouvier-Nave, P., & Ourisson, G. (1984). Distribution of hopanoid triterpenes in Prokaryotes. *Journal of General Microbiology*, 130, 1137-1150.

Rontani, J.-F., & Volkman, J.K. (2005). Lipid characterization of coastal hypersaline cyanobacterial mats from the Camargue (France). *Organic Geochemistry*, 36, 251-272.

Russell, N.J. (1992). Lipids of halophilic and halotolerant microorganisms. In: *The Biology of Halophilic Bacteria* (eds Vreeland RH, Hochstein LI). Boca Raton, CRC Press, pp. 135-161.

Sahoo, S.K., Planavsky, N.J., Kendall, B., Wang, X., Shi, X., Scott, C., Anbar, A.D., Lyons, T.W., & Jiang, G. (2012). Ocean oxygenation in the wake of the Marinoan glaciation. *Nature*, 489, 546-549.

Schidlowski M., Gorzawski H., & Dor I. (1994). Carbon isotope variations in a solar pond microbial mat: Role of environmental gradients as steering variables. Geochimica et Cosmochimica Acta, 58, 2289-2298.

Schidlowski, M., Matizgkeit, U., & Krumbein, W.E. (1984) Superheavy organic carbon from hypersaline microbial mats. Naturwissenschaften, 71, 303-308.

Schinteie, R. (2011). *Ancient life at the extremes: Molecular fossils and paleoenvironmental contexts of Neoproterozoic and Cambrian hypersaline settings*. PhD thesis, The Australian National University.

Schinteie, R., & Brocks, J.J. (2014). Evidence for ancient halophiles? Testing biomarker syngeneity of evaporites from Neoproterozoic and Cambrian strata. *Organic Geochemistry*, 72, 46-58.

1472 Schmerber, G., & Ozimic, S. (1966). *A Petrological Study of the Sediments from Mount Charlotte No.*
1473 *1 Well, Amadeus Basin, Northern Territory*. Bureau of Mineral Resources: Geology and Geophysics,
1474 1966/120.
1475
1476 Schouten, S., van der Maarel, M.J.E.C., Huber, R., & Sinninghe Damsté, J.S. (1997). 2,6,10,15,19-
1477 pentamethylicosenes in *Methanolobus bombayensis*, a marine methanogenic archaeon, and
1478 *Methanosarcina mazei*. *Organic Geochemistry*, 26, 409-414.
1479
1480 Shiea, J., Brassell, S.C., & Ward, D.M. (1990). Mid-chain branched mono- and dimethyl alkanes in
1481 hot spring cyanobacterial mats: A direct biogenic source for branched alkanes in ancient sediments?
1482 *Organic Geochemistry*, 15, 223-231.
1483
1484 Sinninghe Damsté, J.S., Rijpstra, W.I.C., Hopmans, E.C., Prahl, F.G., Wakeham, S.G., & Schouten, S.
1485 (2002a). Distribution of membrane lipids of planktonic crenarchaeota in the Arabian Sea. *Applied*
1486 *and Environmental Microbiology*, 68, 2997-3002.
1487
1488 Sinninghe Damsté, J.S., Schouten, S., Hopmans, E.C., van Duin, A.C.T., & Geenevasen, J.A.J. (2002b).
1489 Cranarchaeol: the characteristic core glycerol dibiphytanyl glycerol tetraether membrane lipid of
1490 cosmopolitan pelagic crenarchaeota. *Journal of Lipid Research*, 43, 1641-1651.
1491
1492 Sinninghe Damsté, J.S., Rijpstra, W.I.C., & Reichart, G.-J. (2002c). The influence of oxic degradation
1493 on the sedimentary biomarker record II. Evidence from Arabian Sea sediments. *Geochimica et*
1494 *Cosmochimica Acta*, 66, 2737-2754.
1495
1496 Skotnicki, S.J., Hill, A.C., Walter, M., & Jenkins, R. (2008). Stratigraphic relationships of Cryogenian
1497 strata disconformably overlying the Bitter Springs Formation, northeastern Amadeus Basin, Central
1498 Australia. *Precambrian Research*, 165, 243-259.
1499
1500 Spear, N., Holland, H.D., Garcia-Veígas, J., Lowenstein, T.K., Giegengack, R., & Peters, H. (2014).
1501 Analyses of fluid inclusions in Neoproterozoic marine halite provide oldest measurement of
1502 seawater chemistry. *Geology*, 42, 103-106.

Stefanova, M. (2000). Head-to-head linked isoprenoids in Miocene coal lithotypes. *Fuel*, 79, 755-758.

Stewart, A.J. (1979). A barred-basin marine evaporite in the upper Proterozoic of the Amadeus Basin, central Australia. *Sedimentology*, 26, 33-62.

Stiehl, T., Rullkötter, J., & Nissenbaum, A. (2005). Molecular and isotopic characterization of lipids in cultured halophilic microorganisms from the Dead Sea and comparison with the sediment record of this hypersaline lake. *Organic Geochemistry*, 36, 1242-1251.

Summons, R.E. (1987). Branched alkanes from ancient and modern sediments: Isomer discrimination by GC/MS with multiple reaction monitoring. *Organic Geochemistry*, 11, 281-289.

Summons, R.E., Brassell, S.C., Eglington, G., & Evans, E. (1988b). Distinctive hydrocarbon biomarkers from fossiliferous sediment of the Late Proterozoic Walcott Member, Chuar Group, Grand Canyon, Arizona. *Geochimica et Cosmochimica Acta*, 52, 2625-2637.

Summons, R.E., Franzmann, P.D., & Nichols, P.D. (1998). Carbon isotopic fractionation associated with methylotrophic methanogenesis. *Organic Geochemistry*, 28, 465-475.

Summons, R.E., Jahnke, L.L., Hope, J.M., & Logan, G.A. (1999). 2-methylhopanoids as biomarkers for cyanobacterial oxygenic photosynthesis. *Nature*, 400, 554-557.

Summons, R.E., Powell, T.G., & Boreham, C.J. (1988a) Petroleum geology and geochemistry of the Middle Proterozoic McArthur Basin, northern Australia: III. *Geochimica et Cosmochimica Acta*, 52, 1747-1763.

Sumner, D.Y. (2001) Microbial influences on local carbon isotopic ratios and their preservation in carbonate. Astrobiology, 1, 57-70.

Suzuki, K.-I., Saito, K., Kawaguchi, A., Okuda, S., & Komagata, K. (1981). Occurrence of *ω*-cyclohexyl fatty acids in *Curtobacterium pusillum* strains. *Journal of General and Applied Microbiology*, 27, 261-266.

ten Haven, H.L., de Leeuw, J.W., Sinninghe Damsté, J.S., Schenk, P.A., Palmer, S.E., & Zumberge, J.E. (1988). Application of biological markers in the recognition of palaeohypersaline environments. In: *Lacustrine Petroleum Source Rocks* (eds Fleet AJ, Kelts K, Talbot MR), Geological Society, London, Special Publications, 40, pp. 123-130.

ten Haven, H.L., de Leeuw, J.W., Rullkötter, J., & Sinninghe Damsté, J.S. (1987). Restricted utility of the pristane/phytane ratio as a palaeoenvironmental indicator. *Nature*, 330, 641-643.

ten Haven, H.L., de Leeuw, J.W., & Schenk, P.A. (1985). Organic geochemical studies of a Messinian evaporitic basin, northern Apennines (Italy). I. Hydrocarbon biological markers for a hypersaline environment. *Geochimica et Cosmochimica Acta*, 49, 2181-2191.

ten Haven, H.L., Rohmer, M., Rullkötter, J., & Bisseret, P. (1989). Tetrahymanol, the most likely precursor of gammacerane, occurs ubiquitously in marine sediments. *Geochimica et Cosmochimica Acta*, 53, 3073-3079.

Thiel, V., Peckmann, J., Richnow, H.H., Luth, U., Reitner, J., & Michaelis, W. (2001). Molecular signals for anaerobic methane oxidation in Black Sea seep carbonates and a microbial mat. *Marine Chemistry*, 73, 97-112.

Thiel, V., Peckmann, J., Seifert, R., Wehrung, P., Reitner, J., & Michaelis, W. (1999). Highly isotopically depleted isoprenoids: Molecular markers for ancient methane venting. *Geochimica et Cosmochimica Acta*, 63, 3959-3966.

Thomas, C., Ionescu, D., Ariztegui, D., & The DSDDP Scientific Team. (2015). Impact of paleoclimate on the distribution of microbial communities in the subsurface sediment of the Dead Sea. *Geobiology*, 13, 546-561.

Tissot, B.P., & Welte, D.H. (1984). *Petroleum Formation and Occurrence*. Springer-Verlag, New York.

Tornabene, T.G., Kates, M., Gelpi, E., & Oro, J. (1969). Occurrence of squalene, di- and tetrahydrosqualenes, and vitamin MK_8 in an extremely halophilic bacterium, *Halobacterium cutirubrum*. *Journal of Lipid Research*, 10, 294-303.

Tornabene, T.G., Langworthy, T.A., Holzer, G., & Oró, J. (1979). Squalenes, phytanes and other isoprenoids as major neutral lipids of methanogenic and thermoacidophilic "Archaebacteria". *Journal of Molecular Evolution*, 13, 73-83.

Turich, C., & Freeman, K.H. (2011). Archaeal lipids record paleosalinity in hypersaline systems. *Organic Geochemistry*, 42, 1147-1157.

Valentine, D.L. (2002). Biogeochemistry and microbial ecology of methane oxidation in anoxic environments: A review. *Antonie van Leeuwenhoek*, 81, 271-282.

van Bentum, E.C., Gert-Jan, R., & Sinninghe Damsté, J.S. (2012). Organic matter provenance, palaeoproductivity and bottom water anoxia during the Cenomanian/Turonian oceanic anoxic event in the Newfoundland Basin (northern proto North Atlantic Ocean). *Organic Geochemistry*, 50, 11-18.

van der Meer, M.T.J., Schouten, S., de Leeuw, J.W., & Ward, D.M. (2000). Autotrophy of green non-sulphur bacteria in hot spring microbial mats: biological explanations for isotopically heavy organic carbon in the geological record. *Environmental Microbiology*, 2, 428-435.

Walter, M.R., Veevers, J.J., Calver, C.R., & Grey, K. (1995). Neoproterozoic stratigraphy of the Centralian Superbasin, Australia. *Precambrian Research*, 73, 173-195.

Wang, R. (1998). Acyclic isoprenoids – molecular indicators of archaeal activity in contemporary and ancient Chinese saline/hypersaline environments. *Hydrobiologia*, 381, 59-76.

Wang, R., & Fu, J. (1997). Variability in biomarkers of different saline basins in China. *International Journal of Salt Lake Research*, 6, 25-53.

West, N., Alexander R., & Kagi, R.I. (1990). The use of silicalite for rapid isolation of branched and cyclic alkane fractions of petroleum. Organic Geochemistry, v. 15, p. 499-501.

Wieland, A., Pape, T., Möbius, J., Klock, J.-H., & Michaelis, W. (2008). Carbon pools and isotopic trends in a hypersaline cyanobacterial mat. *Geobiology*, 6, 171-186.

Wilms, R., Sass, H., Köpke, B., Cypionka, H., & Engelen, B. (2007). Methane and sulfate profiles within the subsurface of a tidal flat are reflected by the distribution of sulfate-reducing bacteria and methanogenic archaea. *FEMS Microbiology Ecology*, 59, 611-621.

Winfrey, M.R., & Ward, D.M. (1983). Substrates for sulphate reduction and methane production in hypersaline sediments. *Applied and Environmental Microbiology*, 45, 193-199.

Wingert, W.S. (1992). GC-MS analysis of diamondoid hydrocarbons in Smackover petroleum. *Fuel*, 71, 37-43.

Sample	Depth	Mineralogy [a]	Sample texture description	Kerogen content (%) [b]	Pr/Ph [c]	Sat [d]	Aro [d]	Sat/Aro
07r011	1566 m	A (0%), D (56%)	Dark grey laminated dolomite interlayered with siliciclastics	0.5	0.90	20.13	1.62	12.43
08r022	1650.8 m	A (90%), D (5%)	Dark brown anhydrite containing fine dark laminae of dolomite	n.d.	1.88	3.37	1.12	3.01
08r011	1651.1 m	A (10.4%), D (84.6%)	Dark grey dolomite interlayered with medium grey anhydrite	0.2	1.37	20.02	3.44	5.82
09r029a	1651.8 m	A (2%), D (95%)	Dark grey dolomite	n.d	0.85	35.49	3.4	10.44
09r029b	1651.9 m	A (86%), D (23%)	Medium grey anhydrite with fine dark laminae of dolomite	n.d	1.00	5.5	1.37	4.01
09r001	1652 m	A (85.2%), D (11.5%)	Predominantly medium grey anhydrite interspersed by thin dark grey dolomite laminae	0.1	0.85	30.21	6.04	5
08r008	1654 m	A (76.8%), D (15%)	Predominantly medium grey anhydrite interlayered by thin dark grey dolomite laminae	0.2	1.25	25.87	8.69	2.98
08r009	1654.5 m	A (56.2%), D (25.9%)	Predominantly medium grey anhydrite interlayered by thin dark grey dolomite laminae	0.5	1.09	113.45	9.99	11.36
08r006	1655 m	A (15%), D (77%)	Dark grey dolomite interlayered with medium grey anhydrite	0.4	1.20	26.72	2.85	9.38
09r004	2113.6 m	A (1.8%), D (77%)	Dark grey dolomite interspersed by siliciclastics and fine laminae of anhydrite	n.d	0.96	40.85	5.75	7.1
07r013	2115 m	A (0%), D (69.9%)	Dark grey laminated dolomite interlayered with siliciclastics	n.d.	0.86	30.59	2.66	11.5

Sample	MAI (%)	MDI (%)	MPI-1	MPR	MPDF	Phen/MP	MDR	9-MP/1-MP	DMDR	TNR-1	TNR-2	MNR	Maturity bracket (R_c)
07r011	n.d.	33	1.18	2.23	0.57	0.3	5.48	1.87	1.39	1.19	0.86	1.23	0.91-1.29
08r022	62	46	0.84	1.30	0.46	0.29	7.54	1.82	0.95	1.35	0.98	n.d.	0.88-1.3
08r011	64	39	1.17	2.16	0.60	0.37	n.d.	1.68	1.67	1.28	0.94	1.30	0.83-1.3

09r029a	51	37	1.37	1.69	0.50	0.22	n.d.	1.78	1.61	1.32	0.92	n.d.	0.85-1.3
09r029b	53	38	1.2	1.74	0.53	0.2	n.d.	1.89	1.58	1.29	0.89	0.91	0.832-1.3
09r001	52	38	1.38	1.75	0.50	0.19	n.d.	1.8	1.62	1.31	0.93	0.87	0.83-1.3
08r008	57	40	1.09	1.53	0.52	0.22	n.d.	1.73	1.67	0.98	0.79	0.89	0.72-1.3
08r009	52	37	0.82	1.64	0.50	0.42	n.d.	2.07	2.47	0.94	0.77	0.93	0.76-1.3
08r006	69	39	1.98	3.99	0.68	0.2	n.d.	2.09	2.76	0.84	0.72	0.96	0.83-1.59
09r004	56	41	1.19	2.10	0.54	0.22	n.d.	1.78	1.21	1.15	0.79	1.39	0.89-1.3
07r013	68	40	1.2	2.05	0.57	0.28	9.21	1.76	1.26	1.16	0.84	1.41	0.9-1.3

Sample	Depth	Kerogen	Av. *n*-alkane [a]	$\delta^{13}C$ (*n*-C_{17}*) [b]	*n*-C_{14}	*n*-C_{15}	*n*-C_{16}	*n*-C_{17}	*n*-C_{18}	*n*-C_{19}	*n*-C_{20}	*n*-C_{21}	*n*-C_{22}	*n*-C_{23}	*n*-C_{24}
07r011	1566	-22.2	-23.8	-0.15	n.d.	n.d.	-24.6	-24.1	-23.3	-22.9	-22.7	-22.7	-23.1	-23.2	n.d.
08r022	1650.8	n.d.	-26.8	-2.4	n.d.	-29.6	-26	-28.6	-26.4	-26.9	-25.9	-25.9	-25.8	-25.7	n.d.
08r011	1651.1	-24.3	-25.3	-0.8	n.d.	-26.7	-25.3	-25.9	-24.9	-24.7	-25	-24.6	-24.8	-24.9	n.d.
09r001	1652	-26.6	-27.1	-1.55	-29.3	-29.6	-28.8	-29.9	-27.9	-26.8	-26.3	-26.4	-26.1	-26.3	n.d.
08r008	1654	-24.1	-25.3	-0.95	-27.9	-27.6	-26.3	-26.8	-25.4	-24.9	-24.3	-24.2	-24	-24.1	n.d.
08r009	1654.5	-26.1	-26.4	-1.6	n.d.	n.d.	-27.9	-29.2	-27.3	-26.9	-25.9	-25.7	-25.3	-25.2	n.d.
08r006	1655	-21.6	-21.9	0.05	n.d.	n.d.	-20.5	-20.6	-20.8	-20.8	-22.5	-23.8	-23.4	-24.5	n.d.

Sample	*n*-C_{25}	*n*-C_{26}	*n*-C_{27}	*n*-C_{28}	*n*-C_{29}	*n*-C_{30}	*n*-C_{31}	*n*-C_{32}	Pr	Ph+Croc	*i*-C_{23}	*i*-C_{24}	*i*-C_{25}+PMI	*i*-C_{37}	*i*-C_{38}	*i*-C_{39}
07r011	-23.4	-23.8	-24.3	-23.8	-24.8	-24.8	-25.6	n.d.	-25	-25.8	n.d.	n.d.	n.d.	n.d.	n.d.	n.d.
08r022	-27	-26.4	-26.7	-27.5	-27.8	-26.3	-25.9	n.d.	n.d.	n.d.	-25.9	-25.8	-24.5	-25.9	-26.4	-25.5
08r011	-25.1	-24.9	-25.1	-25.4	-25.7	-25.9	-26.1	n.d.	n.d.	n.d.	n.d.	n.d.	n.d.	n.d.	n.d.	n.d.
09r001	-25.9	-25.9	-25.9	-25.7	-25.9	-26.5	-26.9	n.d.	-28	-28.9	n.d.	n.d.	-28.1	n.d.	n.d.	n.d.
08r008	-23.9	-24.1	n.d.	n.d.	n.d.	n.d.	n.d.	n.d.	-25.7	-23.9	-24.8	-26.2	-24.7	n.d.	n.d.	n.d.
08r009	-25.2	-25.4	-25.9	-26.5	-26.4	-26.1	-26.2	-26.7	n.d.	n.d.	n.d.	n.d.	n.d.	n.d.	n.d.	n.d.
08r006	-21	-21.2	n.d.	n.d.	n.d.	n.d.	n.d.	n.d.	n.d.	n.d.	n.d.	n.d.	n.d.	n.d.	n.d.	n.d.

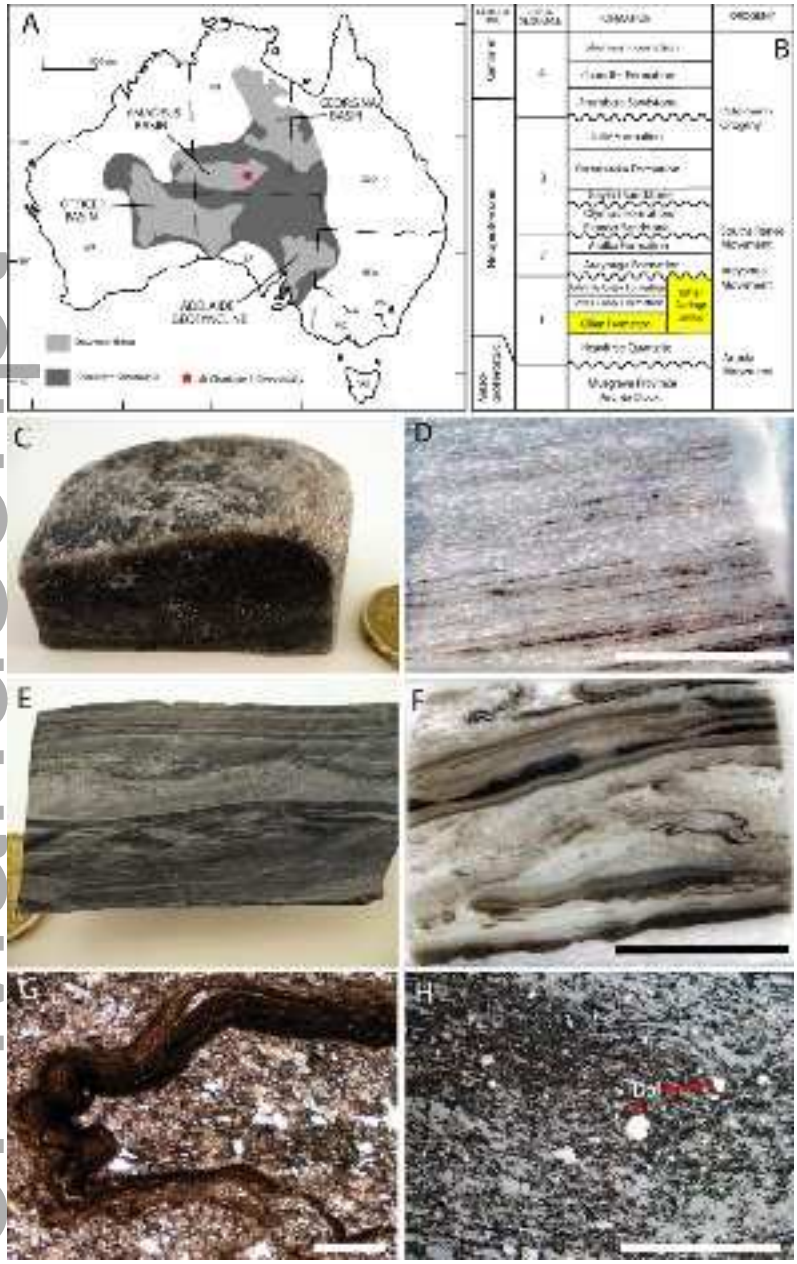

gbi_12245_f1.png

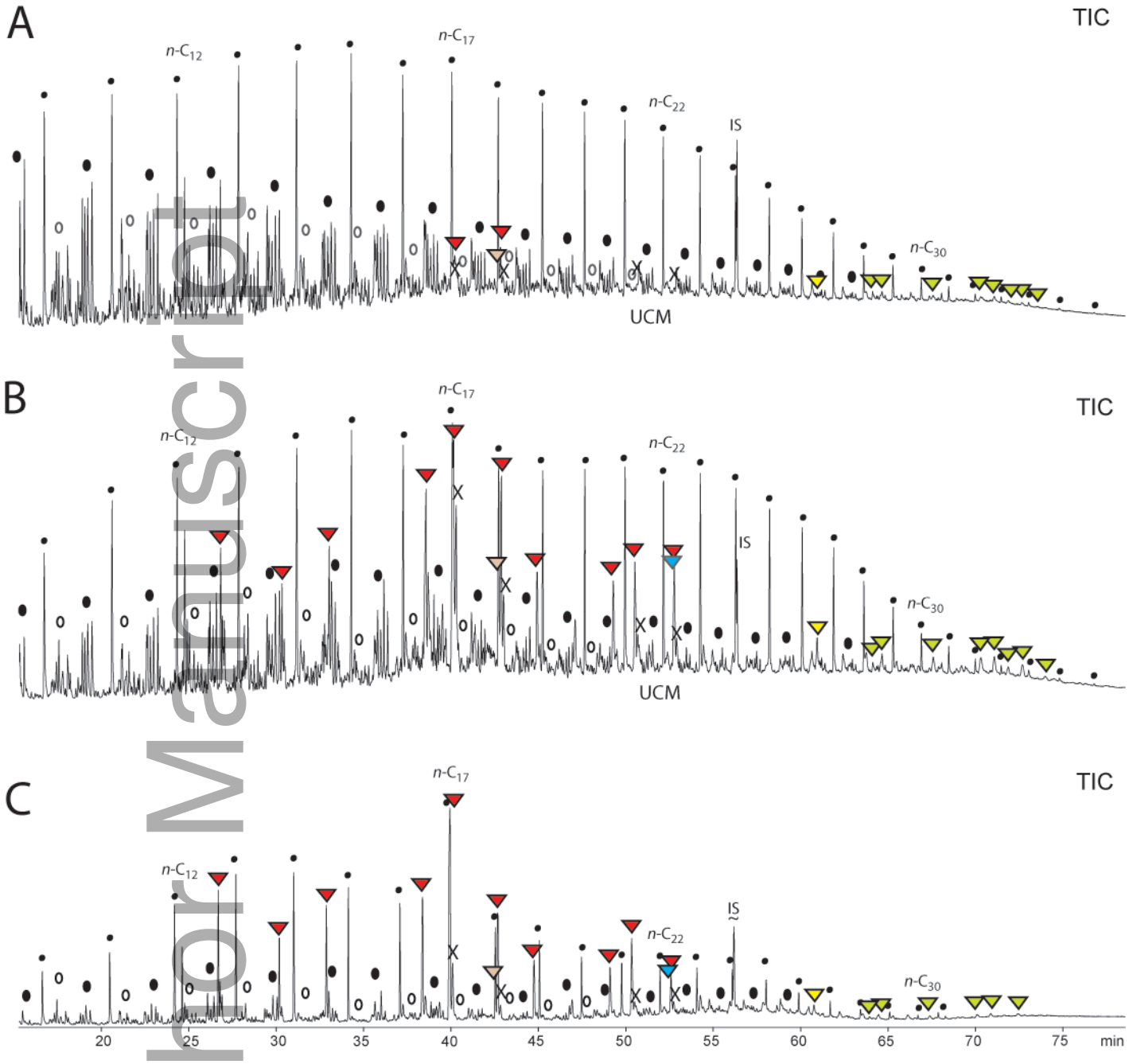

gbi_12245_f2.tif

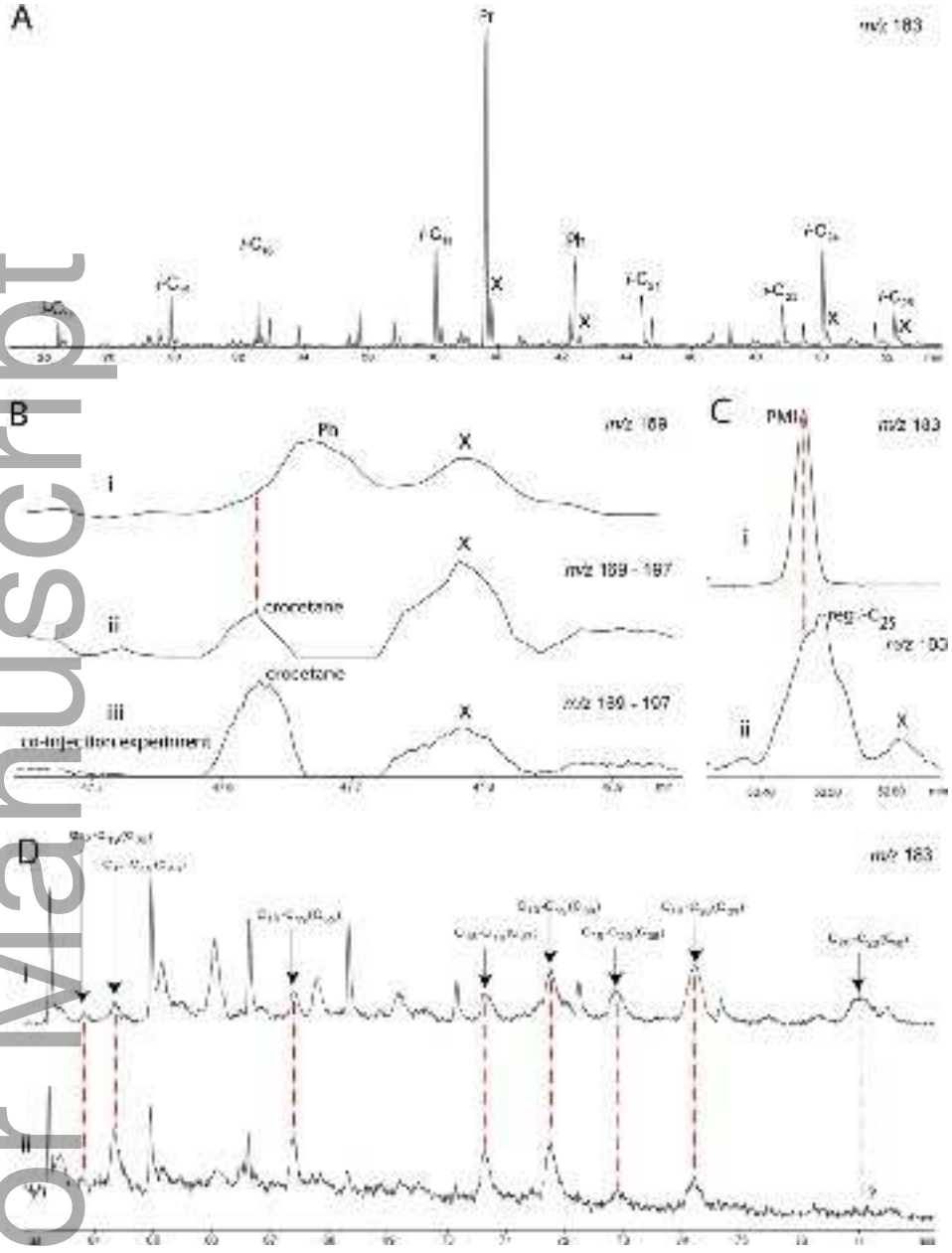

gbi_12245_f3.png

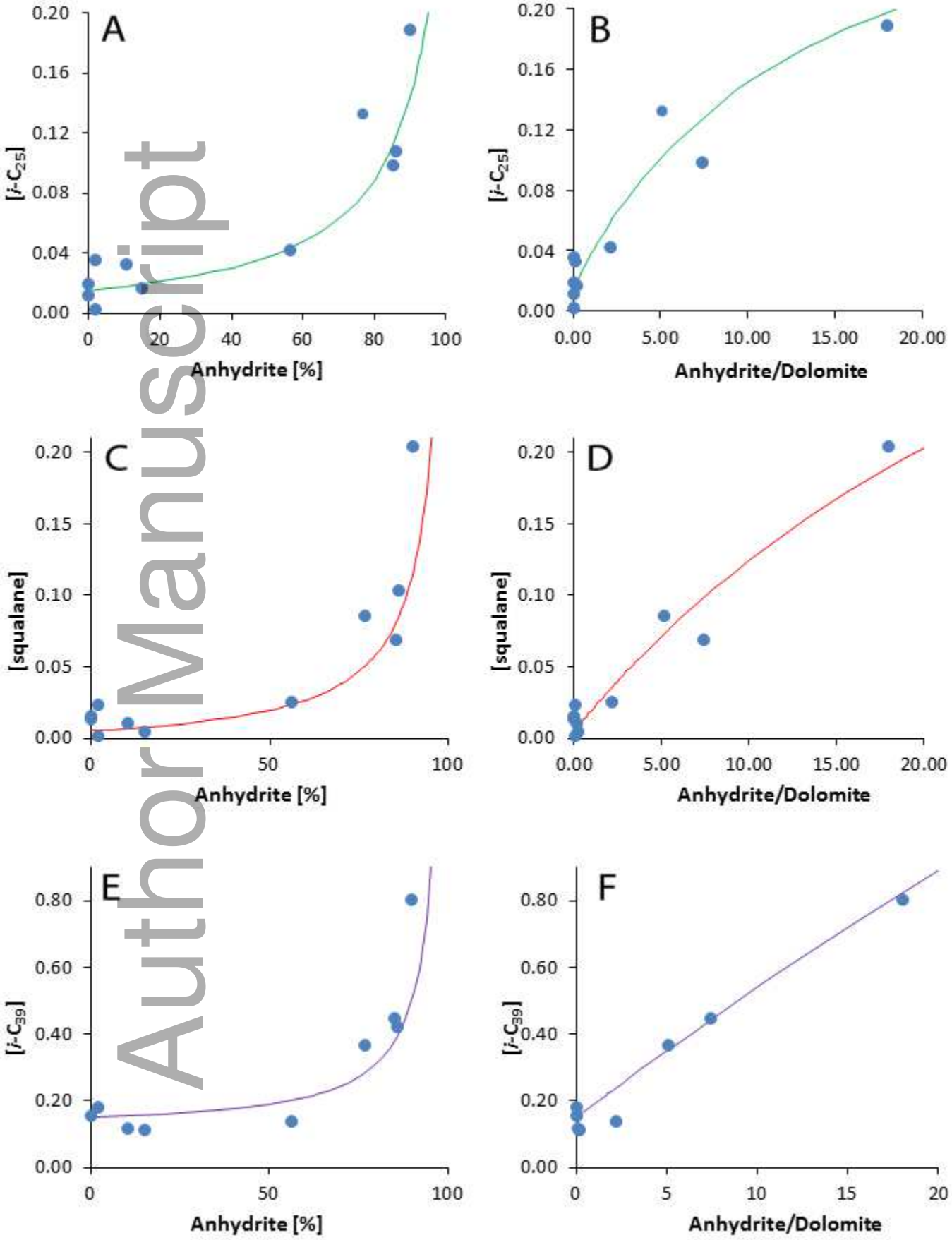

gbi_12245_f4.png

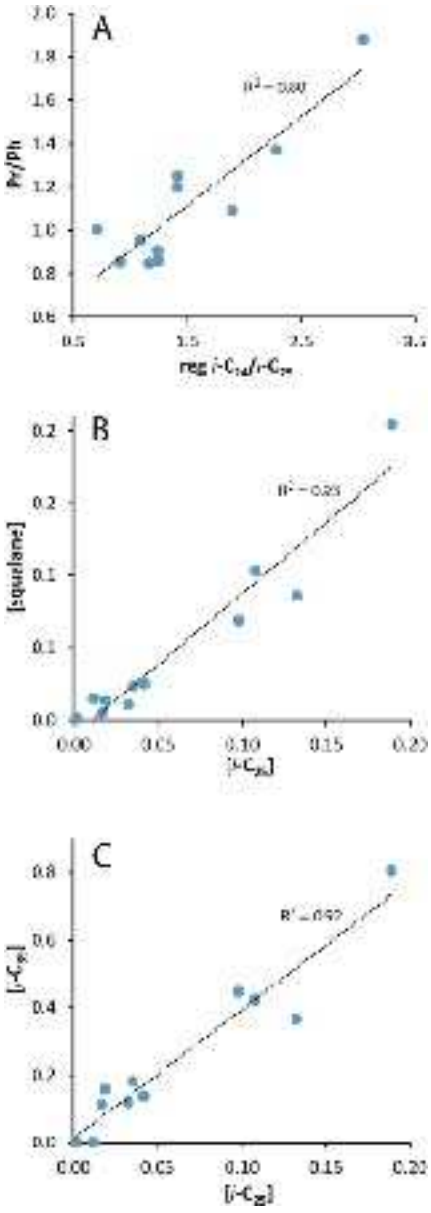

gbi_12245_f5.png

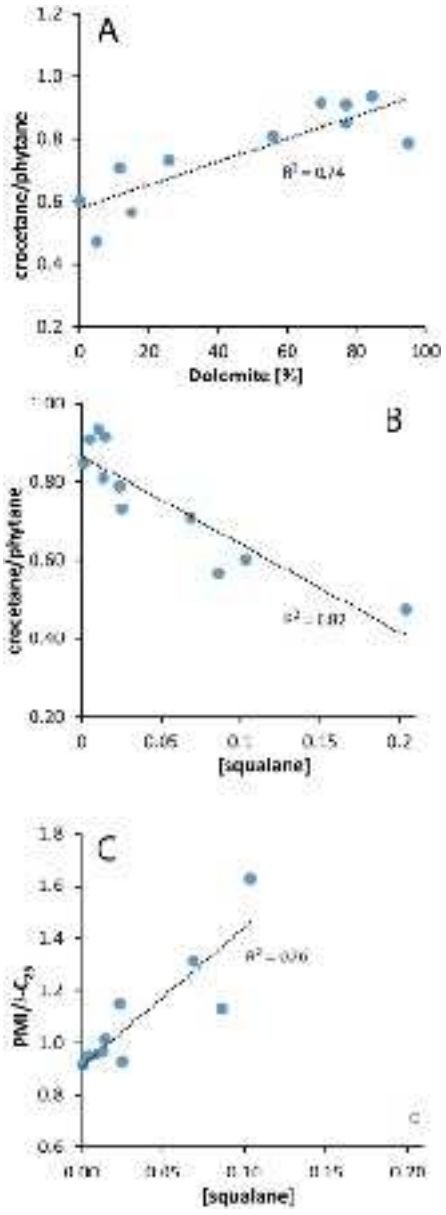

gbi_12245_f6.png

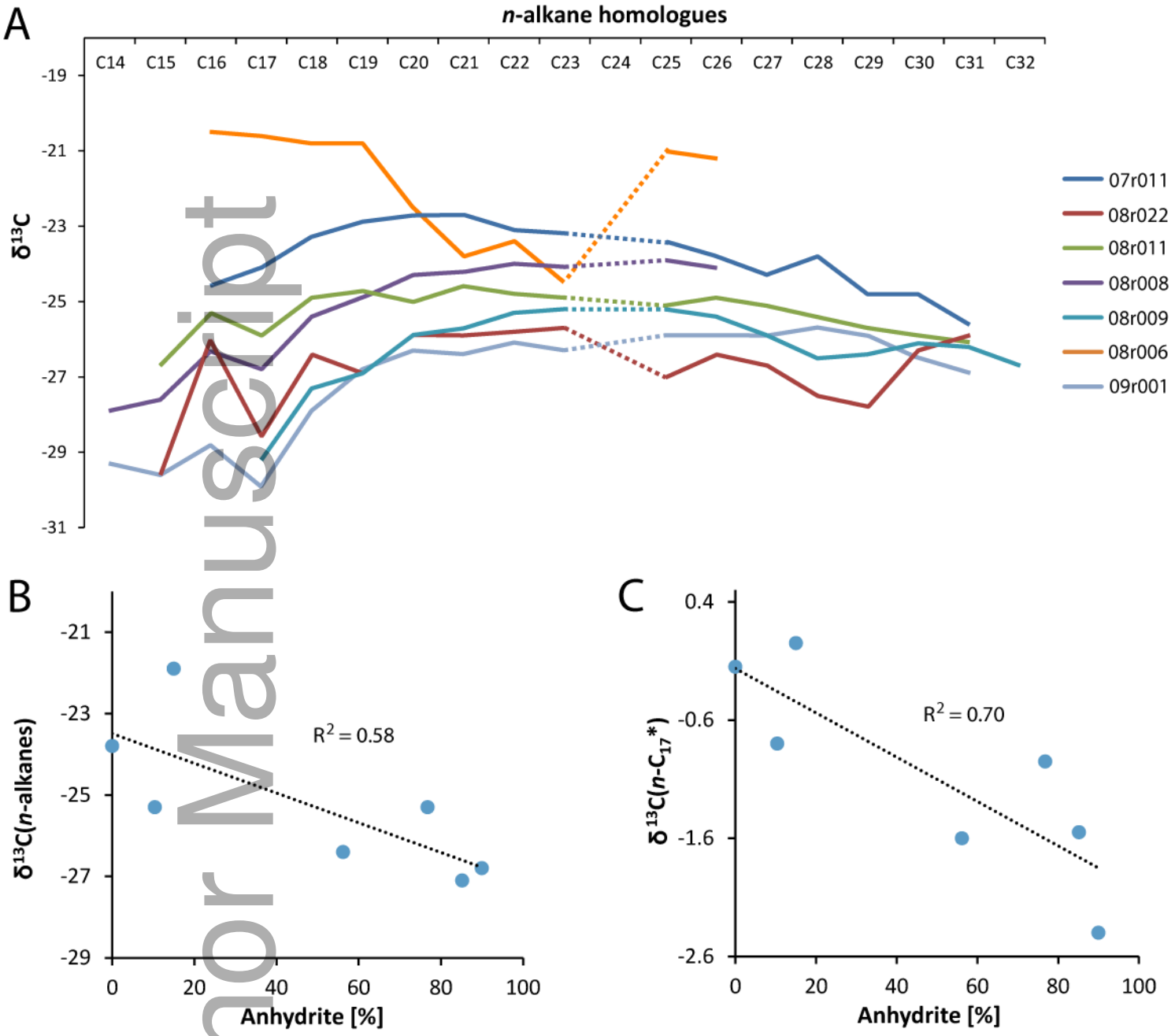

gbi_12245_f7.png